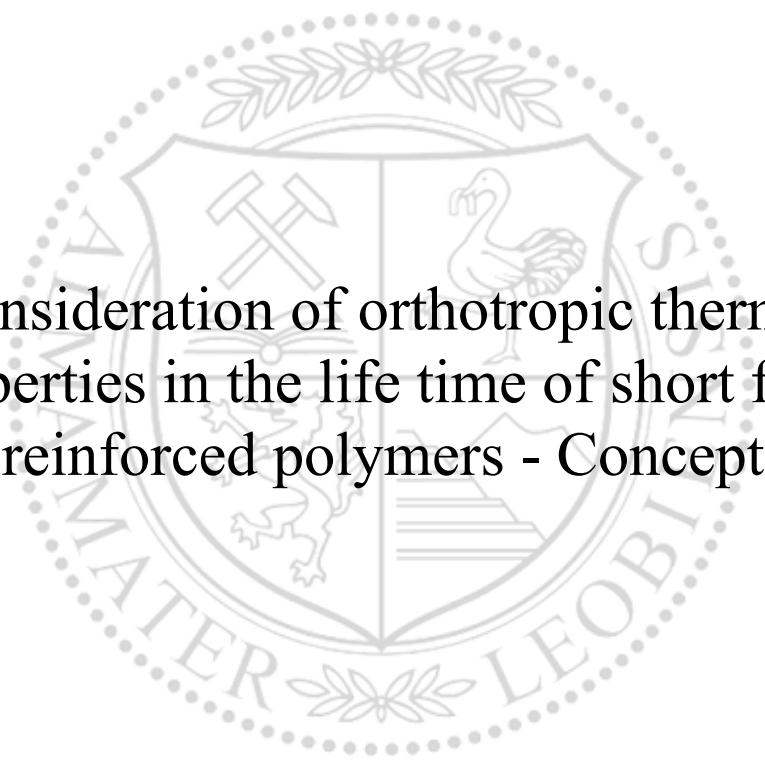




Chair of Automation

Master's Thesis

The background features a large, faint watermark of the University of Leoben seal. The seal is circular and contains a shield with various symbols, including a hammer and pickaxe, a stork, and a lion. The text 'MONTAN UNIVERSITÄT LEOBEN' is visible around the perimeter of the seal.

Consideration of orthotropic thermal
properties in the life time of short fibre
reinforced polymers - Concept

Reza Afsharnia

March 2023



EIDESSTÄTLICHE ERKLÄRUNG

Ich erkläre an Eides statt, dass ich diese Arbeit selbständig verfasst, andere als die angegebenen Quellen und Hilfsmittel nicht benutzt, und mich auch sonst keiner unerlaubten Hilfsmittel bedient habe.

Ich erkläre, dass ich die Richtlinien des Senats der Montanuniversität Leoben zu "Gute wissenschaftliche Praxis" gelesen, verstanden und befolgt habe.

Weiters erkläre ich, dass die elektronische und gedruckte Version der eingereichten wissenschaftlichen Abschlussarbeit formal und inhaltlich identisch sind.

Datum 23.11.2022

Unterschrift Verfasser/in
Reza Afsharnia

Acknowledgement

I would first like to thank my supervisor Dr. Beata Oswald-Tranta, my mentor Prof. Gerald Pinter and my co-supervisor and project manager Dr. Andreas Primetzhofer for giving me the opportunity to work on this interesting topic and for their great supports whenever I ran into a trouble spot or had a question about my research or writing.

I would like to thank also all the colleagues at the Chair of Materials Science and Testing of Polymers and Chair of Automation of Montanuniversität Leoben and Polymer Competence Center Leoben (PCCL), specially DI. Markus Schwaiger, DI. Christoph Tuschl and Dr. Mario Gschwandel for their supports and patience for performing the experimental part of the thesis. I would like to acknowledge our technicians Jürgen Föttinger, Jürgen Grosser and Franz Grassegger for being always helpful.

I am grateful for my family's unconditional, unequivocal, and loving support all the time.

Finally, I must express my very profound gratitude to Dr. Gabriel Stadler for providing me with unfailing support through the process of researching and writing this thesis.

Thank you all!

Zusammenfassung

Diese Masterarbeit beschäftigt sich mit der Entwicklung einer Simulationmethode des thermomechanischen Verhaltens von kurzfaserverstärkten Kunststoffen. In dieser Arbeit wurde eine Multiskalensimulation zur Vorhersage orthotroper thermischer Ausdehnungen in kurzfaserverstärkten Polymeren unter Verwendung der ersten Ordnung Mori-Tanaka-Homogenisierungsschema durchgeführt. Um die Simulation zu evaluieren, wurden mehrere kurzfaserverstärkte Kunststoffe ausgewählt (PP-GF35, PP-GF40, PP-GF50, PA6-GF50, PPA-GF50, PEEK-CF30, PEEK-GF30). Die spezifische Wärmekapazität der ausgewählten kurzfaserverstärkte Kunststoffe sowie ihre Wärmeleitfähigkeit wurden durch verschiedene Tests mittels dynamische Differenzkalorimetrie und Blitzthermographie gemessen. Die thermischen Ausdehnungen der ausgewählten kurzfaserverstärkte Kunststoffe wurden in zwei Richtungen im höchstmöglichen Betriebstemperaturbereich mit einer digitalen Bildkorrelationseinrichtung (DBK) gemessen.

Die höchste beobachtete Abweichung zwischen der Simulation und den Messungen der thermischen Ausdehnungen für PP-basierte Materialien, gehört zu PP-GF35 mit etwa 35% bei 100°C in Querrichtung. Bei PA6-GF50 liegt die maximale Abweichung zwischen Simulation und Messung der thermischen Dehnungen bei 150°C und beträgt etwa 20%. Die höchste Abweichung zwischen simulierten und gemessenen thermischen Ausdehnungen für PPA-GF50 beträgt etwa 29% und tritt bei 120°C auf (bei der Glasübergangstemperatur von PPA). Bei PEEK-GF30 und PEEK-CF30 beträgt die maximale Abweichung zwischen Simulation und Messung der thermischen Ausdehnungen 29% bzw. 40% bei 200°C. Bei beiden PEEK-basierte Materialien wurden jedoch bis zur Glasübergangstemperatur von PEEK keine merkbare Abweichungen festgestellt.

Abstract

This thesis deals with the performing a simulation model for predicting thermomechanical behaviour of short fibre reinforced composites. For this thesis a multi scale simulation has been performed to predict orthotropic thermal expansions in short fibre reinforced polymers, employing Mori-Tanaka first order homogenization scheme. For evaluating the simulation, several short fibre reinforced polymers have been chosen (PP-GF35, PP-GF40, PP-GF50, PA6-GF50, PPA-GF50, PEEK-CF30, PEEK-GF30). The specific heat capacity of the chosen composites as well as their thermal conductivity was measured by performing several differential scanning calorimetry (DSC) and light flash analysis (LFA) test. Thermal strains of the chosen composites have been measured in two directions in the highest possible operating temperature range with an optical digital image correlation (DIC) setup.

The highest observed deviation between the simulation and measurements of thermal strains for PP-Based material, belongs to PP-GF35 with about 35% in at 100°C in transversal direction. For PA6-GF50 the maximum deviation between simulation and measurements of thermal strains occurs at 150°C and is about 20%. The highest deviation between simulated and measured thermal strains for PPA-GF50 is about 29% and occurs at 120°C (around the PPA glass transition temperature). For PEEK-GF30 and PEEK-CF30 the maximum deviation between simulation and measurements of thermal strains are 29% and respectively 40% at 200°C. However for both of the PEEK-Based materials there were no remarkable deviation observed up to the glass transition temperature of PEEK.

Contents

1	Background	2
1.1	Materials	2
1.2	Methods	9
1.2.1	Differential scanning calorimetry (DSC)	10
1.2.2	Thermal conductivity measurement	12
1.3	Digital Image Correlation (DIC)	14
1.4	Mechanical properties-Homogenization	15
1.4.1	Mori Tanaka Theory	16
1.4.2	Coefficient of thermal expansion	16
1.5	Finite Element Method (FEM)	17
2	Experiments	19
2.1	Introduction	19
2.2	Materials	19
2.3	Differential Scanning Calorimetry (DSC)	21
2.4	Flash Light Thermography	23
2.5	Thermal strains	26
3	Simulation	28
3.1	Introduction	28
3.2	Digimat	29
3.3	Abaqus	34
4	Results and discussion	38
4.1	Specific heat capacity	38
4.2	Thermal conductivity	40
4.3	Thermal strain measurements and simulation validation	44
5	Summary and conclusion	47

Introduction

Fabricating parts from various polymeric materials is becoming increasingly common due to their advantages in compare with the usual materials, like lower processing costs, lightweight etc. Thermoplastics are one of the most favorite polymers for industries and they have use in a wide range of products from buttes, and medical devices to automobile and aerospace components. Since thermoplastics have a lower mechanical property in compare with other materials like metals, fiber reinforced thermoplastics were developed to enhance mechanical properties of the thermoplastics. Research shows that long fiber reinforced composites are more disposed to segregation comparing with short fiber reinforced composites. Incorporation of discontinuous fibers into thermoplastics generally yields improvements in mechanical and thermal properties, for instance, stiffness, strength, dimensional stability, service temperature, resistance to creep and fatigue. These improvements are, however, connected with reduced strain (ductility) characteristics and pronounced anisotropy as a result of the structuring of the reinforcement in the molded parts [1].

Nowadays there are several production technologies for short fiber reinforced polymers like, rapid prototyping methods, extrusion etc. in common production methods the distribution of the fibers is highly oriented which causes a significant direction dependency (anisotropy) in thermomechanical properties, as a side effect of enhancing the mechanical properties. Since composite polymers are often used in structures that are operating in a wide temperature range, having an understanding from their behavior under changing temperature is important. In this master thesis a multi scale modeling has been performed, using several software packages, to predict the thermal elongations of short fiber reinforced polymers components.

Chapter 1

Background

This chapter deals with the background of the thesis, firstly polymers and the different types of polymers are introduced. Then the polymers are introduced which are used for the tests. After that the methods, equipment and techniques are explained which are employed for the experiments and the chapter ends up with an overview on the theories which are utilized in the thesis.

1.1 Materials

Thermoplastics, thermosets, elastomers and liquid crystal polymers are the four major form of polymers. The difference between thermosets and thermoplastics is their behavior when they are subjected to heat. Thermosets strengthen when they are heated but they can not be remolded or reheated after initial forming whereas thermoplastics can be reheated or reformed after initial forming without having any chemical changes. In compare with thermoplastics, thermosets can withstand higher operating temperatures, while thermosets are favorite for common usages because of their easier production process, recyclability etc. Nowadays more than 70% of plastic consumption all around the world are thermoplastics [2]. Elastomers are polymers with flexible nature, very high toughness and some other superior properties like abrasion resistance and impermeability [3]. Liquid crystal polymers are a class of polymers which can retain highly ordered structure in a melt or liquid state, which leads to unique mechanical properties, high temperature resistance and excellent thermal stability [4, 5].

At the following are these four polymer types briefly introduced:

Thermoplastics: Thermoplastics have the simplest molecular structure with chemically independent macromolecules, they are softened or melted

by heating, then shaped or formed and solidified by cooling. They could be processed several times and the processing time is short, because it is just a physical reaction. The processing does not release any gases and it is easy to monitor since it is just a physical transformation. From the view point of microstructure, thermoplastics are divided into two categories, **amorphous** and **semi-crystalline** [6].

Amorphous microstructure: In amorphous microstructure, macromolecules are distributed randomly in the polymer, or they are oriented because of the production process, without any relationship with adjacent molecules, see Figure 1.1.1. Amorphous materials do not show a distinct melting point, instead, the material moves from a glassy state to a rubbery state, this transition from glassy state to rubbery state occurs for each polymer in a certain temperature, defined as glass transition temperature (T_g). Below the glass transition temperature, molecules are coiled, entangled and motionless, but above the glass transition temperature the short-range molecular interactions between molecules vanish and they can slip easier, which causes a sudden reduction in E-Modulus, Figure 1.1.3 [6, 7].

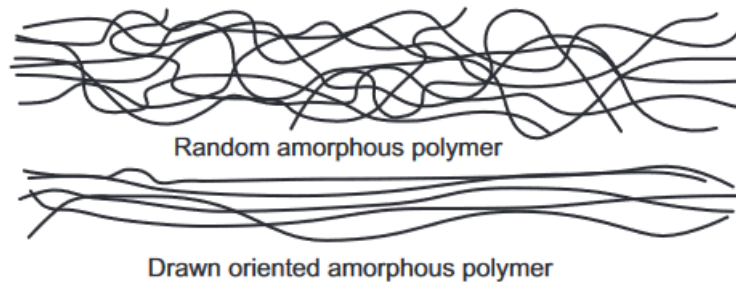


Figure 1.1.1: Microstructure of an amorphous polymer [6]

Semi-crystalline microstructure: In semi-crystalline microstructure, macromolecules are arranged in semi regular small rigid lamellae and the rigid areas are connected to each other with flexible amorphous macromolecules, Figure 1.1.2 shows the schematic microstructure of a semi-crystalline polymer. In semi-crystalline polymers, the modulus drops down by increasing temperature in glass transition range, but in contrast to amorphous polymers, the reduction in modulus is not that much, because in glass transition range just the amorphous part is influenced. Figure 1.1.3, shows the different behaviour of E-Modulus with increasing temperature for amorphous and semi-crystalline polymers [6–9].

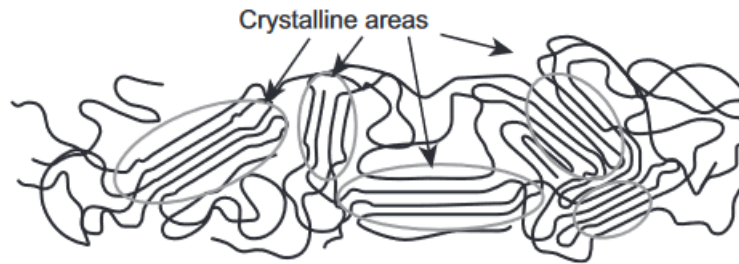


Figure 1.1.2: Microstructure of a semi-crystalline polymer [6]

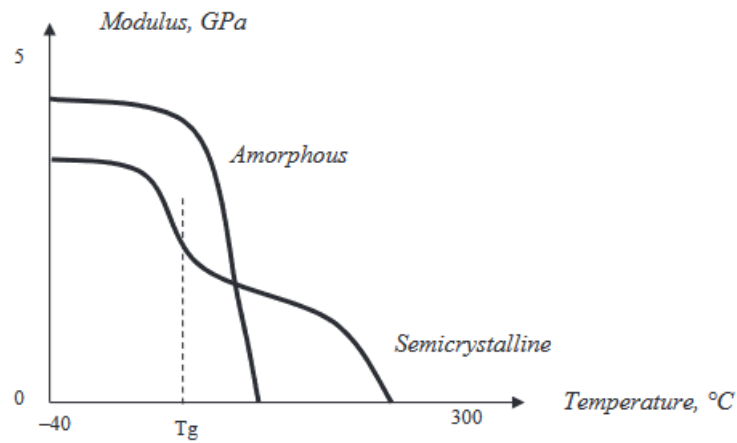


Figure 1.1.3: Schematized E-Module changes vs. temperature for amorphous materials and semi-crystalline materials [9]

Considering the glass transition temperature or the melting temperature, thermoplastic polymers can be classified into three groups: standard, technical and high performance thermoplastics, Figure 1.1.4 shows the maximum allowed operating temperature as well as some examples for each category, considering the microstructure of the polymer [8].

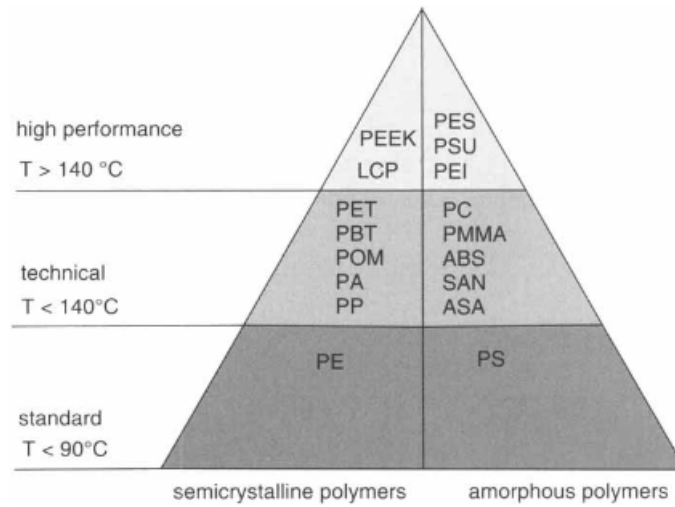


Figure 1.1.4: Classification of the thermoplastics regarding to the maximum allowed operating temperature [8]

Thermosets: A conventional way to distinguish thermoplastics and thermosets is their behaviour when they are heated. Thermoplastics flow when the temperature increases, while thermosets remain solid until degradation temperature [10]. Thermosets are cross-linked polymers and the process of cross-link formation is in thermosets irreversible, curing can occur either by adding curing agent or by heating the material [10, 11].

Elastomers: Elastomers are polymers with flexible nature. Due to their low intermolecular forces they show high degree of elongation and a low E-Module, Figure 1.1.5. Elastomers have amorphous structure with a glass transition temperature lower than the room temperature. The cross-links in the microstructure of elastomers make them possible to regain the original form after deformation [3].

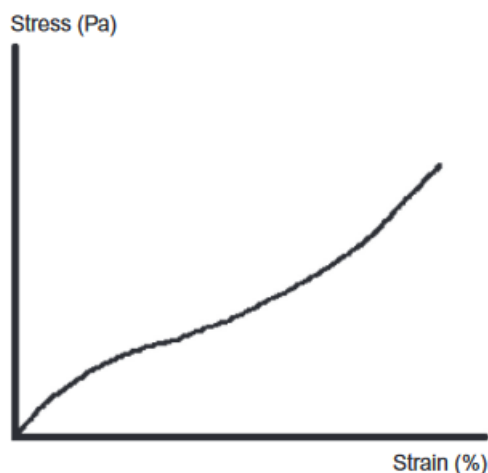


Figure 1.1.5: Typical stress-strain diagram for the elastomers [3]

Liquid crystal polymers: Liquid crystal polymers (LCPs) possess some degree of order in the liquid state. This is achieved by incorporating rigid structural segments into the polymer. These segments will form some order in the liquid state and maintain that order in the solid state. This results in their properties being in between those of liquids and crystalline solids. For example they can have liquid-like flow properties and solid-like tensile strengths and stiffness. Due to the low viscosity in the melt state they are very attractive for thin-wall application and components and due to the high level of order in solid state they provide very high dimensional stability, high strength and rigidity. In general there are two types of LCPs: **Lyotropic** LCPs, which can be produced from solutions, for example dissolving a polymer in a solvent and **thermotropic** LCPs, which can be produced via heating the polymer up to the molten state, Figure 1.1.6 show the schematic microstructure of a thermotropic LCP [4].

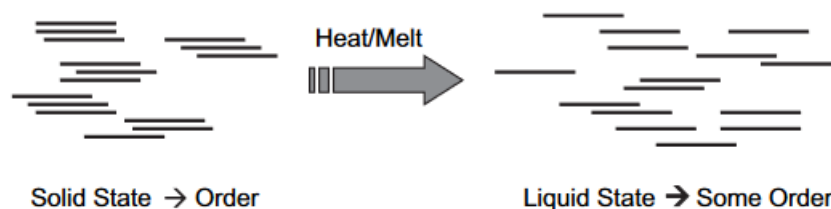


Figure 1.1.6: Schematic of the microstructure of a thermotropic LCP in solid and molten state [6]

The area of interest of this thesis is engineering and high performance

thermoplastics, see Figure 1.1.4. At the following, the investigated thermoplastics in this thesis are introduced in more detail:

Polypropylene (PP) Polypropylene is a thermoplastic polymer with a relatively low melting point ($\sim 170^\circ\text{C}$) and a glass transition temperature of ($\sim -25^\circ\text{C}$). PP is created through polymerization of propylene gas and has many excellent chemical and mechanical properties, such as high softening point, good processability and economic advantages which make it industrially important. The PP market is the second largest polymer business in the world [12–16].

Polyamide 6 (PA6) Polyamide 6 is an important thermoplastic from polyamides family with a melting point around (220°C) and a glass transition temperature of 53°C . PA6 and PA66 are the most popular polyamides since more than 50% of polyamide consumption in industry are PA6 and PA66. PA6 is a product of hexamethylenediamine (6-carbon diamine). PA66 is a product of hexamethylenediamine and adipic acid (6-carbon diacid). The main reasons of choosing PA6 in industry are high temperature and chemical resistance, excellent wear and friction behavior, good heat aging resistance, surface appearance and toughness [17–21].

Polyphthalamide (PPA) Polyphthalamide or High-Performance Polyamide is semi crystalline thermoplastic from PA6 family (PA6T/PA6I). In compare with PA6, PPA has a higher melting point and heat resistance ($T_m = 250^\circ\text{C}$), higher glass transition temperature (135°C), better chemical resistance and higher stiffness [22, 23].

Polyetheretherketone (PEEK) Polyetheretherketone is a semi-crystalline thermoplastic with extraordinary mechanical properties. The Young's Modulus of PEEK is around 3.6 GPa and its melting point is around 350°C and its glass transition temperature around 143°C , PEEK has also excellent chemical resistance as well as excellent wear resistance which makes it a great choice for many commercial applications, from machinery industry to electrical industry and medical devices and dental usages [24–26].

In many cases fillers and reinforcements are mixed with polymer to either enhance the mechanical or thermomechanical properties of the polymer or to reduce the costs.

Fillers and Reinforcements: Fillers are particulate materials, like minerals, diatomaceous earths, talc and etc. The aim of adding fillers to the polymer is just to reduce the costs. The aim of adding reinforcements to the polymers is to enhance the stiffness and strength. Fillers and reinforcements can be in the form of particulates, Platelets or fibres and they can be oriented randomly or aligned in the composite, see Figure 1.1.7. Glass and carbon fibres are the most common reinforcements, they could be added to polymers in large amounts to improve creep resistance, stiffness and geometrical stability, however they can also cause a reduction in impact strength [27,28].

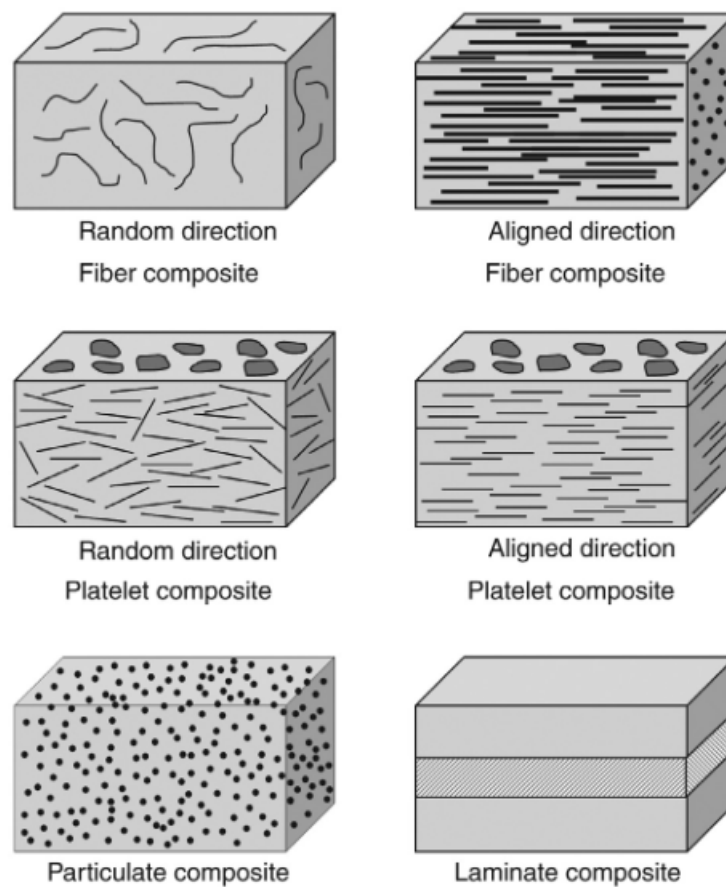


Figure 1.1.7: Several types of composite materials [28]

Short fibre reinforced polymers: Short fibre reinforced composites, are composites containing discontinuous and shorter than a few millimeters long fibres. Often fibre materials are glass or carbon fibre, added to the polymers to enhance the properties of the matrix. Short fibre reinforced composites

have extensively usage in automobile industry, electrical industry, sporting goods, business machines, etc. As a consequence of partial alignment of the fibres, the mechanical and physical properties of short fibre reinforced polymers shows some level of anisotropy, depending on the fibre orientation distribution [28,29]. Typically short reinforcement fibres have a length about 0.22 mm and a diameter about 10 μm .

Injection moulding and extrusion are the most common methods for production components from short fibre reinforced polymers. In the components made using this production methods, the distribution of fibers in the cross section of components is highly nonuniform, due to different flow and temperature condition and can be characterized in two typical forms [30,31].

- Skin-core-skin formation, in this model the thickness of plate will be identified in three regions in terms of fiber orientation, the two outer skin layers with fibers mainly oriented in the mold flow direction and the core layer with mostly oriented fibers in transverse direction of the mold flow, Figure 1.1.8.
- Quasi uniform formation characterizes the fiber orientation in parts with thin cross section, whereby the fibers are mostly in the mold flow direction oriented.

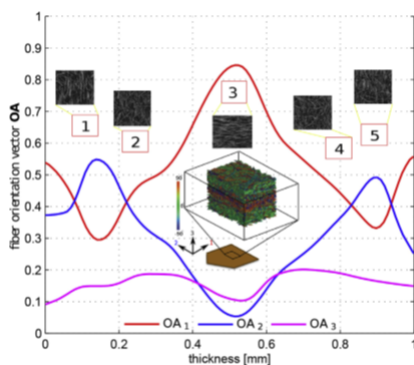


Figure 1.1.8: Fiber distribution in OA_1 : flow direction, OA_2 : transverse to flow direction, OA_3 : thickness [30]

1.2 Methods

To characterize the thermal properties of the chosen materials as well as to measure thermal strains in the prepared specimens, several methods have

been employed. Using differential scanning calorimetry (DSC) method, the specific heat of each composite was measured. To determine the thermal conductivity of each polymer two different devices have been used but with the same principle of working, both methods use namely a light flash test method based on Parker law. Thermal strains have been measured by a Digital Image Correlation (DIC) device at different temperatures. The following section deals with the methods and theories used in the thesis for measuring specific heat, measuring thermal conductivity, measuring thermal strains as well as homogenization computation methods for composites.

1.2.1 Differential scanning calorimetry (DSC)

Principles: Thermal analyses are a family of measurement techniques with a same principle. They measure materials response to being heated or cooled under controlled condition, the aim is to develop a model which can describe the relationship between temperature and a specific physical property of material. There are several methods for thermal analysis, like, DSC, thermogravimetric analysis (TGA), thermomechanical analysis (TMA), dynamic mechanical analysis (DMA), dielectric analysis (DEA), and micro/nano - thermal analysis (μ /n - TA) [32].

Differential scanning calorimetry is the most popular method of thermal analysis. DSC refers to a method which gives quantitative calorimetric information of a sample that is subjected to a simple temperature ramp. According to ASTM E473, DSC is a technique in which the heat flow rate difference into a substance and into a reference is measured as a function of temperature [33]. Figure 1.2.1 shows schematically the internal structure of a DSC device. As it is illustrated in Figure 1.2.1, the temperature of sample and reference crystal are measured by an accurate sensor and two heating elements maintain the sample and reference crystal in the same temperature. The difference in energy needed to bring sample and reference crystal in the same temperature used for calculating thermal capacity of the sample [33].

DSC test provides information about the heat capacity, glass transition temperature, heat capacity jump at the glass transition, melting and crystallization temperatures, heat of fusion as well as thermal history of the material. Figure 1.2.2 indicates exemplary the changes in heat flow recorded by a DSC device during cooling a sample. It shows that for defining the glass transition five temperatures are required. T_b , which is the beginning of the deviation of the DSC curve from linearity, T_1 , the extrapolated onset temperature of the glass transition, T_g , the glass transition temperature, which is the temperature at half - height of the heat capacity decrease, T_2 , the extrapolated end temperature of the glass transition, and T_e , the end

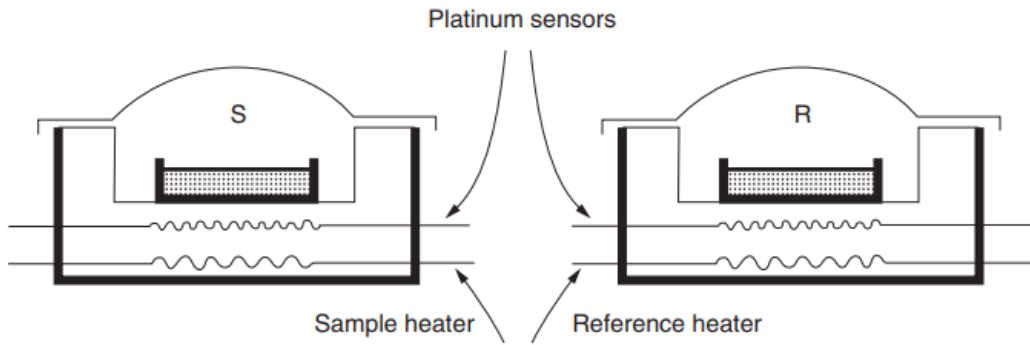


Figure 1.2.1: Working principle of DSC [33]

temperature of the glass transition, where the heat capacity dependence becomes linear again. Heating rate has a pivotal rule in DSC tests and it can vary in a relative wide spectrum, but the most frequently used heating rate is $10^{\circ}\text{C}/\text{min}$ [32].

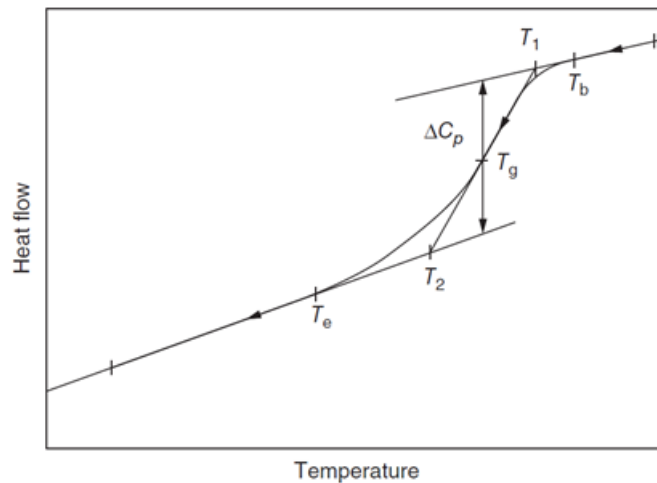


Figure 1.2.2: Characterization of glass transition in DSC test [32]

Specific heat capacity can be calculated using the first law of thermodynamics. Regarding to the first law of thermodynamics, energy cannot be created or destroyed, thus, the changes in internal energy of the system can be written as following [32]:

$$\Delta U = Q + W. \quad (1.1)$$

With: ΔU , the change in internal energy, Q , the heat and W , the work.

For an infinitesimal process Equation 1.1 can be written as following:

$$dU = \delta Q + \delta W. \quad (1.2)$$

Since in the DSC process the only work is volume work Equation 1.2 could be written in the following form:

$$dU = \delta Q + \delta W = \delta Q - pdV. \quad (1.3)$$

then:

$$\Delta U = Q + W = Q - \int_a^b pdV. \quad (1.4)$$

Equation 1.4 can be derived to:

$$\delta Q = dU + pdV = \left(\frac{\partial U}{\partial V}\right)_T dV + \left(\frac{\partial U}{\partial T}\right)_V dT + pdV. \quad (1.5)$$

Which can be rewritten as:

$$\delta Q = \left(\frac{\partial U}{\partial T}\right)_V dT + \left[\left(\frac{\partial U}{\partial V}\right)_T + p\right] dV. \quad (1.6)$$

Since DSC test are performed at constant pressure and volume changes are negligible and there is no external work Equation 1.6 can be written as:

$$dU = \delta Q. \quad (1.7)$$

Then heat capacity at constant pressure can be calculated, using DSC curves (Figure 1.2.2) and Equation 1.8:

$$C_p = \left(\frac{\delta Q}{\delta T}\right)_V. \quad (1.8)$$

To achieve the specific heat capacity, the heat capacity (C_p) should be divided by the mass of the sample.

1.2.2 Thermal conductivity measurement

Heat transfer takes place through three different mechanisms, convection, conduction and irradiation.

For solids the most pivotal mechanism for heat transfer is conduction and the other heat transfer mechanisms in compare with conduction are insignificant [34]. Thermal conductivity is a temperature dependent property of material, which shows the ability of material for transferring heat [35].

In general, there are two major techniques for measuring thermal conductivity, steady-state technique and non-steady-state or transient technique [36]:

- Non-steady-state technique: in this method the data will be recorded during heating up the sample by using transient sensors, comparing with steady-state technique, this method is much faster but less accurate. Flash light thermography, laser flash and hot wire are known non-steady state techniques for measuring thermal conductivity [36].
- Steady-state technique: thermal conductivity of the material will be recorded when temperature difference in whole area used for driving thermal conductivity is constant. This technique provides the most accurate data but it is more time demanding in compare with the non-steady-state method. Some of the most common steady-state techniques are heat flow meter, comparative, pipe method and direct heating [36].

The suitable technique could be chosen regarding to desired temperature interval for measuring thermal conductivity and desired accuracy as well as the investigated material [36].

Flash light thermography: Flash light thermography is a non-steady-state technique for measuring thermal conductivity of the material.

In this method the flash lamp flashes once, the light will be absorbed by the front face of the specimen and it will cause a thermal gradient between front face and rear face, thus heat flows in the thickness direction and simultaneously an IR-camera/sensor is recording the temperature of the rear face of the specimen. Figure 1.2.3 illustrates the schematic of flash light thermography setup. Figure 1.2.4 shows a schematic of recorded data from IR-camera

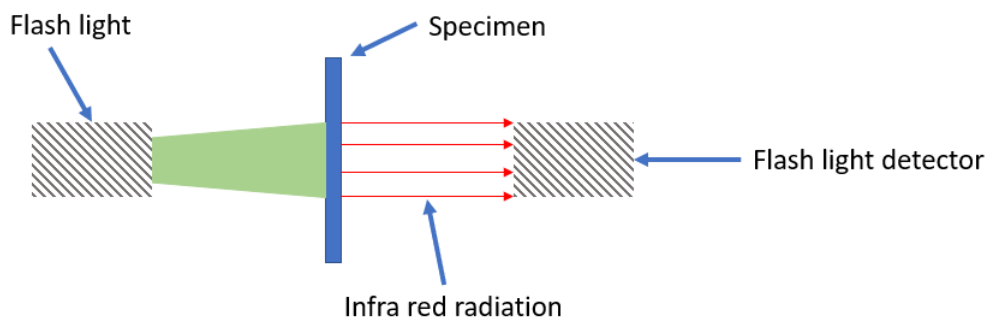


Figure 1.2.3: Flash light thermography setup

in flash light thermography, this graph shows how thermal diffusivity, κ , can be calculated according to Parker law [37], Equation 1.9.

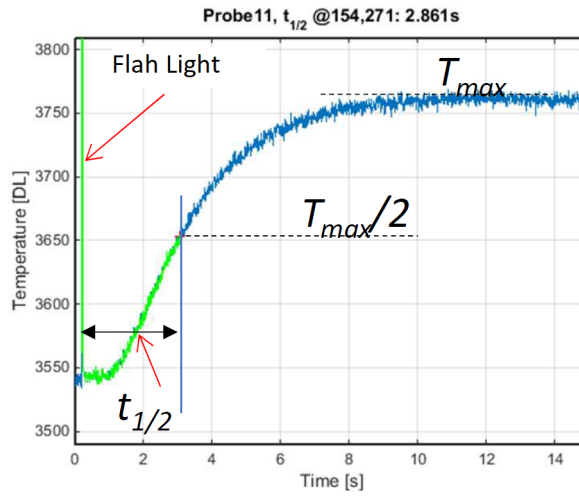


Figure 1.2.4: Exemplary recorded data by IR-camera

$$\kappa = \frac{\lambda}{\rho \cdot c} = \frac{1.38 \cdot d^2}{\pi^2 \cdot \frac{t_1}{2}}. \quad (1.9)$$

With:

κ : thermal diffusivity

λ : thermal conductivity

ρ : density

c : specific heat

d : specimen thickness

$t_{\frac{1}{2}}$: time to achieve half of the maximum temperature on the rear surface

1.3 Digital Image Correlation (DIC)

DIC is an innovative non-contact optical technique for measuring strain and displacement. DIC works by comparing photos of the component or the specimen at different stages of deformation. By tracking blocks of pixels, the system can measure surface displacements and build up a full field 2D or 3D deformation vector fields and strain maps. For DIC, it is important that pixels are randomly and unique and have a certain level of contrast and intensity [38].

1.4 Mechanical properties-Homogenization

The aim of homogenization for heterogeneous materials is to find an equivalent material, which has an equivalent effective macro stiffness as the primary heterogeneous material. Figure 1.4.1 illustrates the linear elastic homogenization idea for a material with two different phases having different stiffness (C_0 and C_1). The goal is to calculate an equivalent stiffness \bar{C} , which fulfills Hook's law [39].

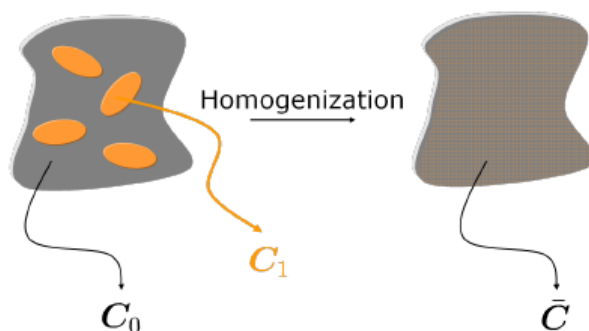


Figure 1.4.1: The idea of homogenization in linear elasticity [39]

For short fibre reinforced polymers, mechanical and thermomechanical properties are affected by the following parameters, which should be taken into account for homogenization [29]:

- properties of components,
- fibre-matrix interfacial adhesion strength,
- fibre volume fraction,
- fibre orientation distribution and
- fibre length distribution.

There are several approaches for homogenization of nonhomogeneous materials like Halpin–Tsai model [40], Mori-Tanaka model [41] and etc. [42]. The Mori-Tanaka model is very successful in predicting the effective properties of two phase composites. In theory, Mori-Tanaka model can predict the properties of composites up to a moderate volume fraction of fibres (about 25% volume fraction) but in practice it predicts the properties even beyond this range reasonably [39]. The Mori-Tanaka model is an approximate use of Eshelby's solution [43] for single inclusion problem. Unlike single inclusion

problem, multi-inclusion does not have an analytical solution and whole of the homogenization models for multi-inclusion composites are based on single inclusion problem with different assumptions [39].

1.4.1 Mori Tanaka Theory

Mori-Tanaka model expresses the mechanical behaviour of the composite in terms of the average strain and average stress, Equation 1.10 [42]:

$$\langle \sigma \rangle = C \langle \epsilon \rangle \quad (1.10)$$

Where the effective average elastic modulus $[C]$ is given by Equation 1.11:

$$C = (V_m C_m + V_f C_f A)(V_m I + V_f \langle A \rangle)^{-1} \quad (1.11)$$

With:

V_m and V_f : volume fractions of the fiber and the matrix

C_m and C_f : fourth order elasticity tensor of the fibers and the matrix

A : relates average strain ϵ_f and ϵ_m through the Equation 1.12,

$$\epsilon_f = A \epsilon_m \quad (1.12)$$

Where: ϵ_f and ϵ_m are the average strain in fiber consequently in the matrix.

1.4.2 Coefficient of thermal expansion

The coefficient of thermal expansion (CTE) is defined as the change in the linear dimension of the body per unit change of temperature. CTE of short fibre reinforced composites can be calculated for three cases regarding to the fibre orientations, unidirectional fibre orientation, partially misaligned fibre orientation and randomly fibre distribution [44]. In practice most of the components from short fibre reinforced polymers are produced by a mold injection or an extrusion method with a partially misaligned fibre orientation [44]. In [44] is explained that, the coefficient of thermal expansion of short fibre reinforced polymers with a partially misaligned fibre orientation can be calculated as a function of fibre length distribution $f(l)$, fibre orientation distribution $g(\theta)$, fibre volume fraction and the elastic properties of the fibre and matrix based on theory of Schapery. Equation 1.13 and Equation 1.14 show the analytical method for calculation of coefficient of thermal expansion

in short fibre reinforced polymers in the main direction and transverse to the main direction [44]:

$$\alpha_1 = \int_{\theta=0}^{\phi/2} \int_{l=0}^{\infty} (\alpha_1^0 \cos^2(\theta) + \alpha_2^0 \sin^2(\theta)) f(l) g(\theta) dl d\theta \quad (1.13)$$

$$\alpha_2 = \int_{\theta=0}^{\phi/2} \int_{l=0}^{\infty} (\alpha_1^0 \sin^2(\theta) + \alpha_2^0 \cos^2(\theta)) f(l) g(\theta) dl d\theta \quad (1.14)$$

α_1^0 and α_2^0 are defined in Equation 1.15 and 1.16:

$$\alpha_1^0 = \frac{E_f \alpha_f V_f + E_m \alpha_m V_m}{E_f V_f + E_m V_m} \quad (1.15)$$

$$\alpha_2^0 = (1 - \nu_f) \alpha_f V_f + (1 + \nu_m) \alpha_m V_m - \alpha_1^0 (\nu_f V_f + \nu_m V_m) \quad (1.16)$$

Where:

E_f and E_m : Young's modulus of the fibres and the matrix

α_f and α_m : the CTE of the fibres and the matrix

V_f and V_m : volume fraction of the fibres respectively volume fraction of the matrix

ν_f and ν_m : poisson ratio of the fibres respectively poisson ratio of the matrix.

1.5 Finite Element Method (FEM)

Finite element method is specially eligible for complex geometries. When using the finite element method, the problem domain will be discretized into a set of small numbered elements, connected together through numbered nodes, using a so called meshing procedure [45]. To calculate the displacements in each element, the displacements in each node of the element should be calculated and then the displacement in the whole element can be driven from the calculated nodal displacements [45].

The elements can be either linear or non-linear. In a linear element, displacements between nodes change linearly with the distance between nodes. In higher order elements displacements between the nodes are interpolated with a higher order polynomial. In general a non-linear element type is suggested, when the geometry experiences large deformation, material is non-linear or when there is a contact between components which can cause local deformation, because non-linear elements need significantly more solution effort in compare with linear elements [45, 46].

For three dimensional geometries there are two types of elements, hexahedral and tetrahedral. In comparison with hexahedral, tetrahedral has several advantages: great flexibility in fitting complex geometries, unique linear interpolation from vertices to interior and ease of refinement [47].

If the material properties defined in the simulation is temperature dependent, a coupled thermomechanical simulations is necessary for predicting the behaviour of material. In coupled thermomechanical simulation elements have one more degree of freedom than normal, which is dedicated to temperature [48].

Chapter 2

Experiments

2.1 Introduction

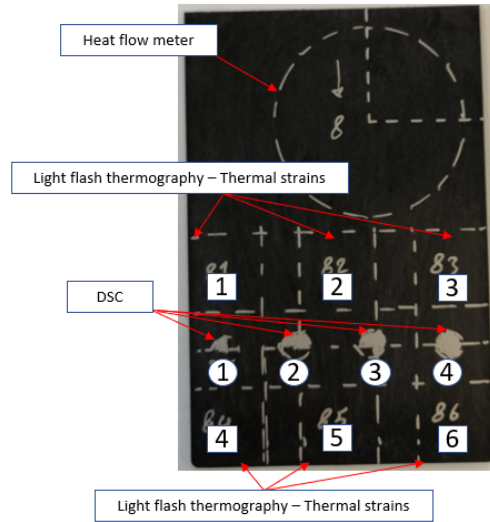
This chapter deals with the materials and testing strategies, which have been used for this thesis. In this master thesis seven different short fibre reinforced polymers have been investigated. Table 2.1.1 indicates the composite content regarding to the supplier announcement. The delivered materials from the suppliers was in the form of the injection moulded plates with a dimension of $120 \times 80 \times 2$ mm ($L \times W \times H$). According to the size requirements for each test, specimens were processed and prepared from the primary plates, Figure 2.1.1 illustrates the geometry of plates as well as the location and dimension of the specimens for each test.

Table 2.1.1: List of the chosen composites for this thesis

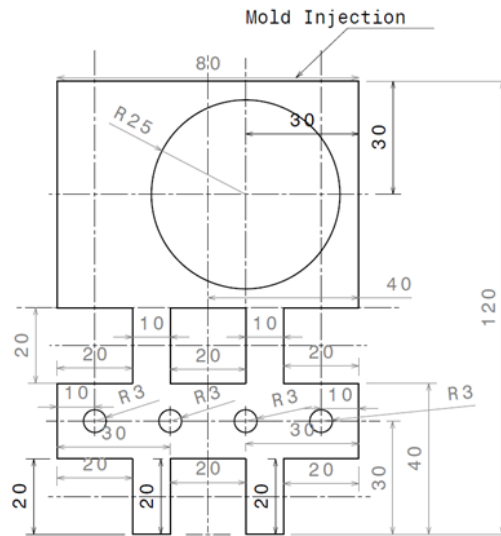
Plate Nr.	Matrix	Fiber	Fiber Weight fraction (%)	Notation
1,2	Polypropylene	Glass	40	PP-GF40
3,4	Polyphthalamide	Glass	50	PPA-GF50
5,6	Polyamide 6	Glass	50	PA6-GF50
7,8	Polypropylene	Glass	50	PP-GF50
9,10	Polyetheretherketone	Carbon	30	PEEK-CF30
11,12	Polypropylene	Glass	35	PP-GF35
13,14	Polyetheretherketone	Glass	30	PEEK-GF30

2.2 Materials

Table 2.1.1 listed, seven different composites in this thesis have been investigated. Three of the materials are Polypropylene with different amount of



(a) Injection moulded plates with the sketch of test specimens



(b) Dimensions and position of the samples for DSC, heat flow meter and light flash thermography test as well as the samples for measuring thermal strains

Figure 2.1.1: Schematic of the test samples location

glass fibre, two of them are Polyetheretherketone once with glass and once with carbon fibre and finally from Polyamide 6 and Polyphthalamide just one representative with 50 wt.% was chosen. At the following each of the composites and their most common usage in industry are introduced:

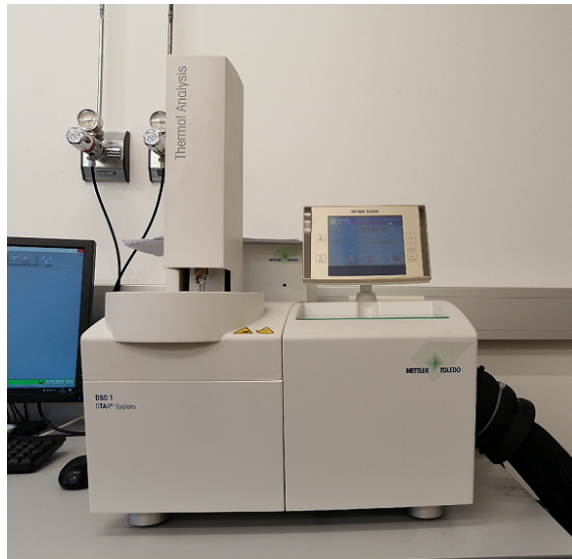
- **PP-GF35, PP-GF40 and PP-GF50:** Are chemically coupled high performance short glass fibre reinforced polypropylene compound intended for injection moulding, they are especially demanded by automobile industry for producing front end carriers, structural parts, under the bonnet components, tank hinges as well as pedal carries [49]. The PP-base materials used in this for the thesis was provided by **Borealis® GmbH**.
- **PA6-GF50:** PA-GF50 has widely application in automobile, electrical and industry as well as in consumption goods [50]. The investigated material was provided by **EMS Grilon®**.
- **PPA-GF50:** The material was provided by **EMS Grivory®**. PPA-GF50 is widely used in automobile industry(in fuel system, internal and external parts etc.), in electrical industry and in household appliance [51].
- **PEEK-CF30:** Short carbon fibre reinforced PEEK shows very high mechanical properties and tends to be less abrasive than glass fibres, which results in improving wear and friction properties. PEEK-CF30 has application in many industries like automotive, marine, nuclear, down hole oil, electronics and aerospace [52]. The PEEK-CF30 material for this study was provided by **Evonik® GmbH**.
- **PEEK-GF30:** This type of composite is ideal for conditions, which require to withstand long-term static loads at high temperature and for components which work in an extreme environment. Some of typical components made from PEEK-GF30 are: Rollers, Gears, insulators etc. [53]. The investigated material was provided by **Evonik® GmbH**.

2.3 Differential Scanning Calorimetry (DSC)

As mentioned in Section 1.1, plates produced by injection moulding method shows a level of inhomogeneity in fibre orientation distribution, therefore to minimize the effect of the sample position in the test and achieving result, which are representative for the whole plate, for each material, DSC test was



(a) Weighting the prepared samples for DSC tests



(b) Used Mettler Toledo DSC 1 for DSC measurements

Figure 2.3.1: Used equipment for (a) weighting DSC samples and (b) for performing DSC tests

performed for two different samples from two different positions on the initial plates, once on the side and once in the middle of the plate (position 1 and position 2, see Figure 2.1.1), and further, for the simulation, the mean value of these two measurements is considered. After extracting DSC samples with a diameter of 6 mm from the moulded plates, their weight should be modified to nominal value of 25 mg, since the reference crystal of the DSC device has a weight of 25 mg. Because the primary weight of the stamped DSC samples was several times higher than what it should be, the samples were sanded from one side to achieve the desired weight. The weight of the samples after modification is varying from 19.12 mg to 25.05 mg, Figure 2.3.1a. The DSC device used for the measurements was **DSC1** from **Mettler Toledo**[®], see Figure 2.3.1b, and the heating and cooling rate was set on $10\text{ }^{\circ}\text{C min}^{-1}$. For each material was a temperature interval chosen, similar to the maximum nominal operating temperature interval of the polymer. Specific heat measurements were carried out during both heating and cooling process. Chosen temperature interval for Polypropylene base composites was from $-25\text{ }^{\circ}\text{C}$ up to $150\text{ }^{\circ}\text{C}$ and for other materials from $-40\text{ }^{\circ}\text{C}$ up to $200\text{ }^{\circ}\text{C}$.

Moreover for verifying the measured specific heat capacity, the specific heat of the fibre and matrix materials for room temperature have been ex-

Table 2.3.1: Literature value of heat capacity for Matrix and Carbon/Glass Fiber

Material	Specific heat C_p ($J.g^{-1}.K^{-1}$)
PP	1.58 [55]
PA6	1.44 [54]
PPA	1.4 [56]
PEEK	1.05 [57]
Glass fiber	0.8 [58]
Carbin fiber	0.75 [59]

tracted from the literature and from internet sources, see Table 2.3.1. The specific heat of each composite have been calculated regarding to it's content, using the equation 2.1 [54]:

$$C_P = C_{p1}X_1 + C_{p2}X_2 + \dots + C_{pi}X_i \quad (2.1)$$

Where:

C_{pi} is the specific heat capacity of the pure component i in the mixture and X_i is the mass fraction of the component i .

The literature value of specific heat capacity in room temperature for the matrix materials as well as for glass and carbon fiber are illustrated in table 2.3.1.

2.4 Flash Light Thermography

Flash light thermography for this thesis have been performed, employing two different devices, once with the light flash thermography, available at the chair of Automation of Montanuniversity Leoben at room temperature, and once using the **LFA 467 Hyperflash[®] - Light Flash Apparatus** provided by **Polymer Competence Center Leoben GmbH (PCCL)** which can provide thermal conductivity as a function of temperature in an temperature interval from -100°C to 500°C .

Thermal conductivity measurements at room temperature: As mentioned earlier, for measuring the thermal conductivity at room temperature, the setup at the chair of Automation have been used. The setup is equipped with a flash light providing 6000 J energy in a duration of $(1/1150)s$ and a

VELOX 1310k SM IR-camera, Figure 2.4.1 shows the setup of the equipment. The procedure of measurement starts when the user pushes the flash light button and then the thermocamera records the temperature changes on the rear face of the specimen. The recorded data by the thermocamera should be processed at the next step in **Matlab**[®] in an arbitrary area of the specimen, defined by the user (see green square on Figure 2.4.2), in order to determine the thermal diffusivity of the specimen. Thermal conductivity could be derived from thermal diffusivity (see section 1.2.2 Equation 1.9).

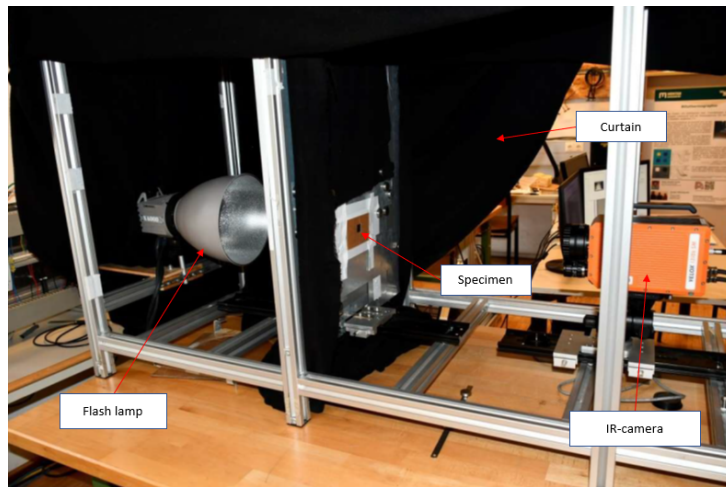


Figure 2.4.1: Flash light thermography setup

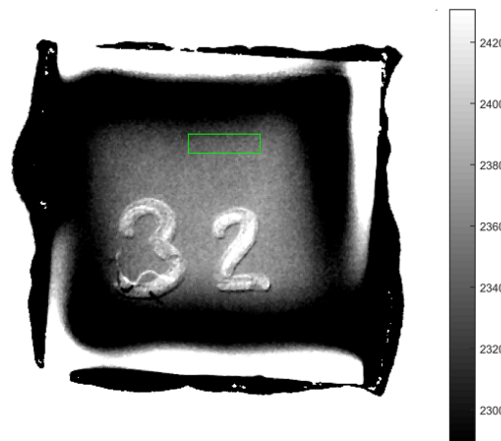


Figure 2.4.2: Flash light thermography specimen and the chosen area for calculating thermal diffusivity (green square)

Flash Light Thermography was performed four times for each material,

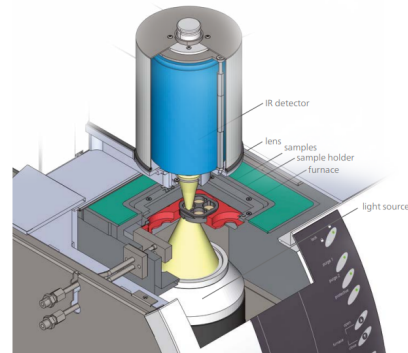
on the other word, sample 1 and sample 2 (see Figure 2.1.1) from two different plates of the same material were investigated. The aim of repeating the tests on more samples and from different places is to investigate the homogeneity in different plates and in different places. For the samples with bright color (PEEK-GF30) it was necessary to cover the sample with a thin layer of graphite to prevent light transmission through the sample which could cause significant errors in the measurements. It should also be considered that the thermal conductivity of the covering layer is included in measurements, but it could be neglected since the thickness of the color layer it too small. For samples with dark primary colors spraying graphite had no effect on the measurement and coating the sample with a layer of graphite is not necessary.

Thermal conductivity measurements as a function of temperature:

The temperature depending thermal conductivity measurements have been performed using the LFA 467 Hyperflash apparatus at PCCL. In each round the device can measure thermal diffusivity of 16 specimens and the principle of work is the same like flash light thermography method, but an IR-detector, rather than thermocamera, records the temperature changes on the rear face of specimen, see Figure 2.4.3. Based on the experiences for achieving reasonable results the samples should be covered with a very thin layer of carbon , for this aim whole of the samples have been painted, using a graphite paint spray.



(a) The LFA 467 Hyperflash device used for thermal conductivity measurements [60]



(b) LFA 467 Hyperflash principle of working [60]

Figure 2.4.3: Flash light thermography (a) setup and (b) principle of working

Temperature depending thermal diffusivity measurements have been performed for four different samples from two different places on the plates. Sample 1 and sample 3, Figure 2.1.1, from two different plates of the same

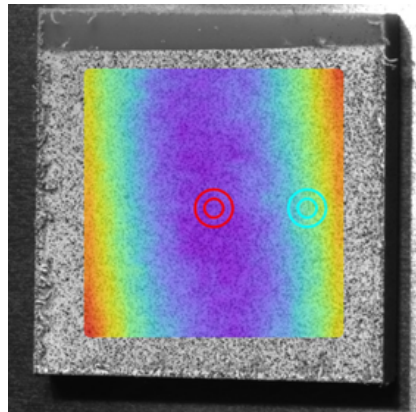
material have been investigated. The tests have been performed in a temperature range from $-40\text{ }^{\circ}\text{C}$ up to $200\text{ }^{\circ}\text{C}$ with temperature steps of $40\text{ }^{\circ}\text{C}$ for all of the materials except PP. For PP the investigated temperature interval was from $-25\text{ }^{\circ}\text{C}$ up to $150\text{ }^{\circ}\text{C}$ with temperature steps of $25\text{ }^{\circ}\text{C}$. The aim of choosing different samples for light flash thermography is to compare if the results from both methods are similar and to investigate if the plates from the aspect of thermal conductivity are homogenous.

2.5 Thermal strains

Thermal strains have been measured by **DanTec[®]Solid Mechanics DIC** available at PCCL, Figure 2.5.1a, which measures thermal strains based on **Digital Image Correlation (DIC)** method. The apparatus measures thermal strains in two directions (thermal strains in the thickness direction are not taken into account), utilizing an optical setup with two cameras. Since the device uses an optical method for measuring thermal strains, it is necessary to create a reference pattern on the specimens before starting the measurement. Due to the time consuming nature of these tests, the test have been performed for each material just once on the sample number 2, Figure 2.1.1. The starting temperature of the tests for all materials, except PP, was $-40\text{ }^{\circ}\text{C}$ and temperature was increased step-by-step up to $200\text{ }^{\circ}\text{C}$ with an increase of $10\text{ }^{\circ}\text{C}$ in each step. The investigated temperature interval for PP was from $-25\text{ }^{\circ}\text{C}$ to $150\text{ }^{\circ}\text{C}$ with the same temperature increase in each step. The changes in the pattern have been recorded with the cameras and afterwards user can calculate the thermal strains in an arbitrary area on the specimen, Figure 2.5.1b. Regarding to the device producer the chosen area should be as wide as possible to optimize the statistical calculations of the measurements.



(a) Used DanTec - Solid Mechanics DIC device for measuring thermal expansions [61]



(b) An example for the samples used for thermal expansion investigation and user defined representative area for calculating thermal strains(colored square)

Figure 2.5.1: Thermal expansion measurements (a) the device used for the measurements and (b) an specimen subjected to the investigations

Chapter 3

Simulation

3.1 Introduction

The aim of this chapter is to develop a multi-scale model, which can predict the thermal expansions of short fibre reinforced polymers, considering the microstructure properties, like fibre orientation and fibre length etc. For this thesis two software packages have been used, firstly **Digmat[®]** was employed for micro-mechanical modelling of the investigated composites, considering Pre-phase material properties and microstructure information (Digmat-MF). Digmat-MAP transferred mesh data from injection molding simulation (Process mesh) to the developed **Abaqus[®]** model (Structural mesh) to obtain an optimal mesh. In the last step, Digmat-CAE combined calculated material properties from Digmat-MF with the mapped mesh orientation data from Digmat-MAP to create required mesh and material data in an appropriate format for Abaqus, the working flow in this software is illustrated in the Figure 3.1.1.

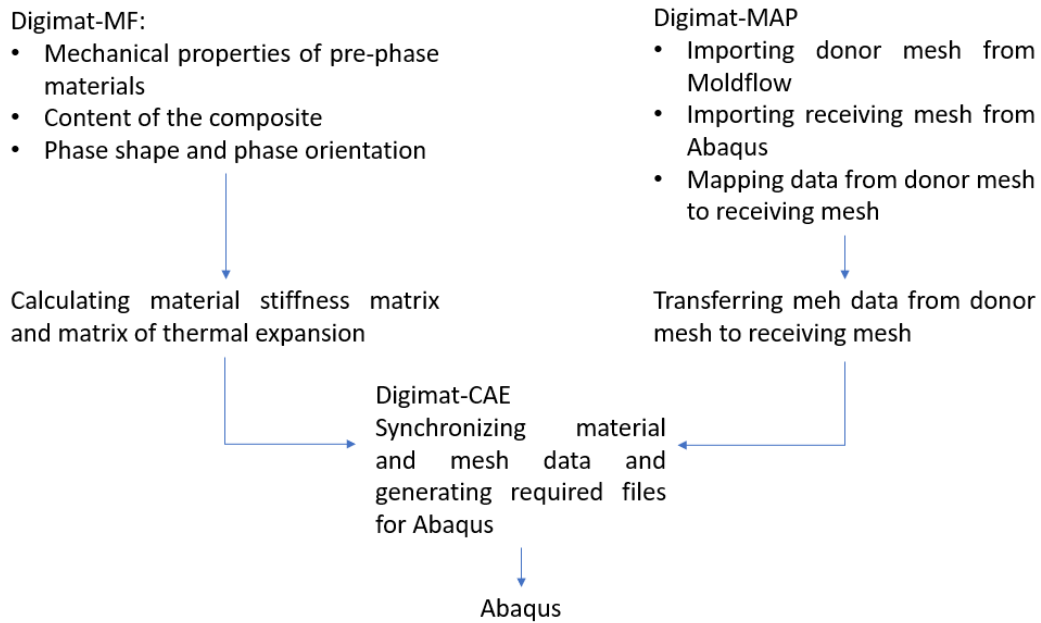


Figure 3.1.1: Working flow in Digimat

Utilizing calculated material properties of the polymers and the results from light flash analysis as well as the results from differential scanning calorimetry, an Abaqus Simulation have been performed for predicting the thermal expansions in each one of the polymers.

Following are the simulation process in Digimat and respectively in Abaqus explained:

3.2 Digimat

As mentioned in section 1.4, simulating material behaviour in the scale of microstructure will be computationally prohibitive. To reduce the computational efforts of simulation, using the so called homogenization methods could be helpful. The task of homogenization is to calculate a stiffness matrix for the heterogenous material, based on the pre-phase material properties and the microstructure information, which behaves most likely to the heterogenous material. For calculating the homogenized stiffness matrix of the investigated material, as well as transferring fibre orientation data from processing mesh to the structural mesh three different modules of the software package Digimat have been used. Following is the simulation procedure in Digimat explained.

Digmat-MF: In this module physical and mechanical properties of the pre-phase materials as well as microstructure information of the composite are to define, there are several types of analysis but in this study thermo-mechanical analysis is desired, since changes in mechanical properties of the materials with temperature are not negligible. By definition, all of the investigated materials in this thesis are heterogenous, since they are consisting of a matrix material and a conclusion phase, which in this case are the short fiber reinforcements. A mean field homogenization with first order Mori-Tanaka scheme, see section 1.4.1 is applied for homogenization of the composites, which is very successful method for predicting equivalent stiffness of two-phase composites with less than 25 – 30% volume fraction of inclusions [39], see Figure 3.2.1.

Units System : Undefined

Analysis type

Mechanical

Thermomechanical

Thermal

Electrical

Mean Field homogenization:

Homogenization scheme: Mori-Tanaka Double inclusion

Homogenization order: First order

Linearization method: Incremental

Multi-inclusion homogenization: Multi-step method

Figure 3.2.1: Digimat-MF general parameters

At the next step, thermomechanical properties of the pre-phase materials should be defined. Table 3.2.1 illustrates the thermomechanical properties of the matrix and fiber materials. In the investigated temperature interval,

Table 3.2.1: Thermomechanical properties of the matrix and fibre materials

Material	Density (g/mm^3)	Young's modulus (MPa)	Poisson ratio	Coefficient of thermal expansion ($\times 10^{-5}$)
PP	0.0009	2000	0.43	9.7
PA6	0.00118	3000	0.39	6
PPA	0.0011	3317	0.4	5.4
PEEK	0.00128	3800	0.38	5
Glass Fibre	0.0025	76000	0.22	1
Carbon Fibre	0.00175	300000	0.27	0.23

Young's modulus of the matrix materials is changing significantly, especially around glass transmission temperature (T_g), as mentioned in section 1.1,

which must be considered for the simulation, for this purpose a piecewise linear function has been defined for each matrix material in Digimat, Figure 3.2.2. It should be noted that the changes in Young’s modulus for the carbon and glass fibers in the intended temperature interval are negligible [62, 63]. For PP-base composites, the temperature dependent coefficient of thermal expansion was provided by the supplier and it has been taken into account by defining a piecewise linear function over the investigated temperature interval.

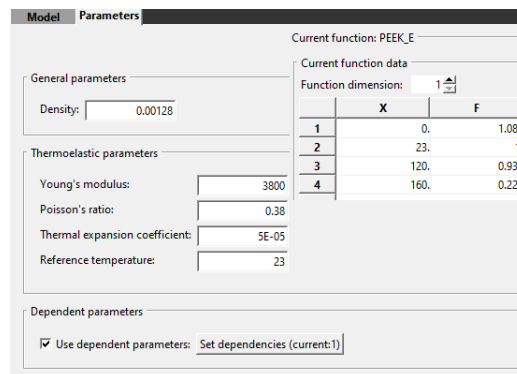


Figure 3.2.2: Piecewise linear function for describing PEEK Young’s modulus temperature dependency

Material definition should be followed by characterization microstructure of the composite. In this step the fibre mass fraction, aspect ratio, fibre radius as well as fibre orientation are identified, Figure 3.2.3. Aspect ratio for the investigated composites except PP-base composites is 30 regarding to the earlier studies [31], respectively regarding to the producer announcement, for PP the aspect ratio is 40 defined.

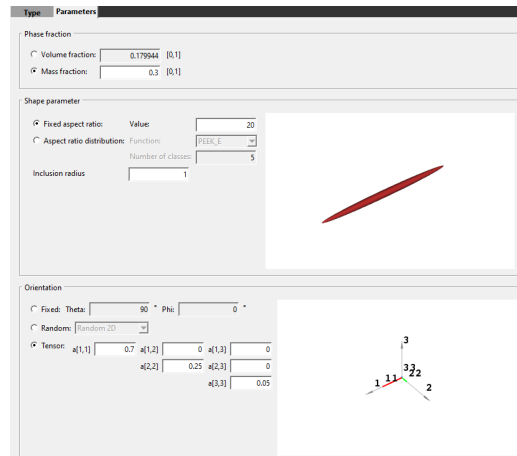


Figure 3.2.3: Inclusion parameters for PEEK-30GF

Due to the single layer structure of the polymers the representative volume element (RVE) module can be skipped, and it is not necessary to define damage for the case of this thesis. Just in loadings module the operation temperature is defined from -40°C to 200°C respectively for Polypropylene from -25°C to 150°C .

Digmat-MAP Due to the complex shape of the moulds and also due to the numerical advantages the mesh type in moulding simulation composed to be triangles for 2D simulation and tetrahedrons for 3D simulation [64,65]. Whereas, for structural simulation for example hexahedral mesh provides better results. Mesh mapping allows to profit having different mesh types for processing and structural simulation by transferring the processing data to the structural mesh. Processing data can include fibre orientation, residual stresses, porosity etc [39]. In this study just the fibre orientation data should transferred to the structural mesh. For this aim Digimat-MAP needs the two following meshes:

- **Donor mesh**, which carry the orientation tensor field
- **Receiving mesh**, which will receive the information from Donor mesh

In this study Donor mesh is an injection molding simulation performed in **Moldflow**[®] based on Fogar-Tucker orientation equation, which is already provided from the last projects. The Donor mesh contains only the fibre orientation data in form of a 3×3 symmetric tensor and the information is stored at the integration points of the mesh, after transferring orientation information from donor mesh to receiving mesh, the element's orientation

is constant and is defined at the center of the element [39, 64]. Receiving mesh is a 20×20 mm square with 2 mm thickness, discretized with cubic structural elements, developed in Abaqus. The part with processing mesh should be translated to the desired positions, as shown in Figure 2.1.1, and mapping process should be executed for each positions once, to transfer fiber orientation data to the structural mesh. Figure 3.2.4 shows the simulated primary plate in Moldflow (donor mesh) and the black spot in the middle of the plate shows the structural mesh created in Abaqus.

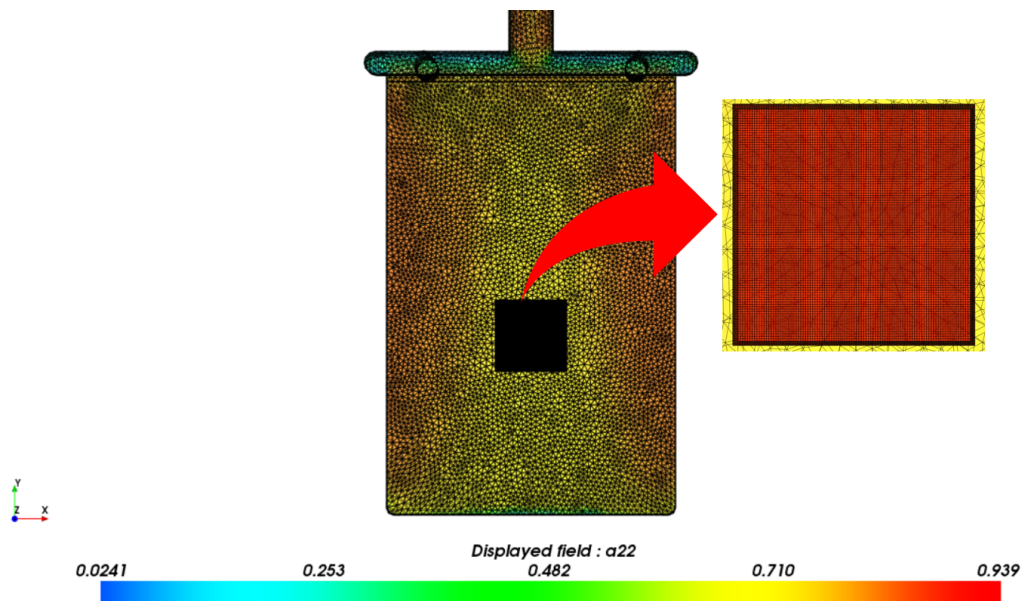


Figure 3.2.4: Digimat-MAP, Donor mesh and the structural mesh placed on it (red spot)

Since for PP-base materials the fibre orientation matrix is provided by the producer, mesh mapping step could be skipped for these composites. For PP-base composites material simulation in Digimat-MF has been performed three times with three different fibre orientation matrix and further in Abaqus for these composites a three-layer model is implemented and for each layer a different material is defined.

Digmat-CAE Digimat-CAE is a tool to bridge the gap between processing simulations and structural finite element analysis. This tool transfers data from processing simulation to the structural analysis per element, considering all of the effects from processing simulation e.g. fiber orientation, residual stresses, temperature field etc. which makes an accurate material

and structural multi-scale modelling possible. In Digimat-CAE the following three main solutions are provided for performing a multi-scale simulation:

- Micro solution
- Hybrid solution
- Macro solution

following these three solutions are briefly discussed.

Micro solution, uses strong multi-scale coupling techniques. In this method, Digimat interactively computes material properties and communicates with the structural code at each iteration of the overall computation. Micro solution is suitable for different kind of anisotropic, temperature/strain dependent material behavior [39].

Hybrid solution, uses weak multi-scale coupling techniques for calculating the material properties. For this solution, Digimat pre-computes macroscopic material properties to communicate with the structural code at each iteration of the computation. Hybrid solution is based on the reduction of the material model to the computation of the macroscopic material properties. The most important advantage of the hybrid simulation in compare with Micro simulation is lower computation load on the CPU and therefore less time demanding simulations [39].

Macro solution, uses weak multi-scale coupling techniques for linear material properties. For Macro solution, Digimat pre-computes macroscopic material properties which are then used in structural code for each iteration during whole computation process [39].

In this thesis hybrid solution is employed to which provides a reasonable compromise between accuracy and efficiency. In this module, the material properties are imported from Digimat-MF and mesh data is imported from Digimat-MAP, other parameters remain unchanged in this module. The output of this step is 4 files with **.aba**, **2×.log** and **.mat** format, which are required later for the simulation in Abaqus.

3.3 Abaqus

After generating a $20 \times 20 \times 2$ mm 3D deformable sample in part module in Abaqus, in property module, material and mesh data should be imported from Digimat. For importing material properties from Digimat, there are two possible ways, the material properties and orientation data could be called by Abaqus, using the Digimat Plug-in, as shown in Figure 3.3.1, or it could be done manually by creating a new material and defining the material

Simulation

properties according to the **.aba** file, created by Digimat-CAE in the previous step, see Figure 3.3.2.

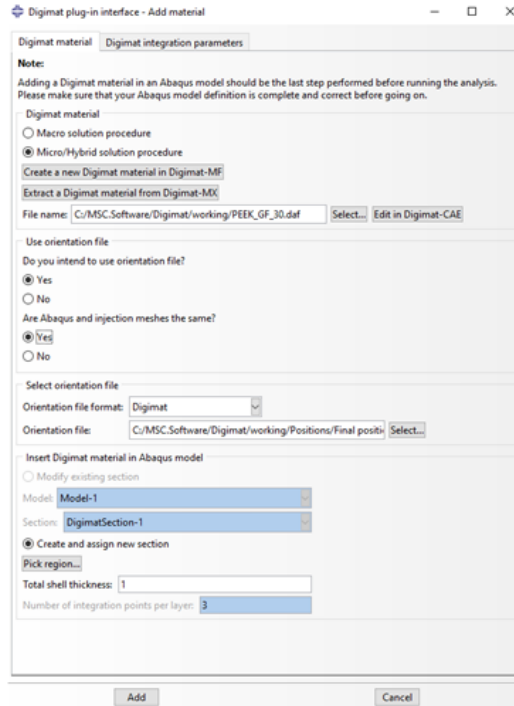


Figure 3.3.1: importing material properties to Abaqus using Digimat Plug-in

```

** DIGIZABA 2021.2 - 01/09/2021 18:09:20
** Depending on the element type, one or two of these commands may be needed.
***TRANSVERSE SHEAR STIFFNESS
**The following transverse shear stiffness is computed for a unit thickness shell
***It's an estimation of this stiffness based on the shear modulus of the stiffest material in the composite
***This estimation is based of the formula : (5/6).G_33.(thickness), (5/6).G_23.(thickness), 0.0
***In order to compute an accurate estimate one must use the shear modull of the composite (which can be computed by Digimat).
**1606.83, 1535.61, 0.
**HOURGLASS STIFFNESS
*** The following hourglass stiffness are only estimates based on
*** Please refer to ABAQUS documentation in order to compute accu
**9.64085, 5.79852
**MATERIAL, NAME = PEEK_GF_30
**DENSITY
0.00149953
**USER MATERIAL, TYPE = MECHANICAL, CONSTANTS = 1
0
**DEPVAR, delete=9
9

```

← Density
← User Material - Mechanical Constants
← Depvar

Figure 3.3.2: required data from **.aba** file, for defining the material properties in Abaqus

Additionally thermal conductivity and specific heat of each material as a function of temperature from the LFA and DSC measurements should be added to the material properties.

For PP-base composites, as mentioned earlier, a three-layer model (skin-core-skin model) was implemented in Abaqus by making three partitions in the direction of thickness. Each of the skin layers has a thickness of 0.2 mm and the core has a thickness of 1.6 mm. In the property module, for each layer one different material has been created, regarding to the simulations which have been already performed for each layer in Digimat, and each material was assigned to the corresponding layer. Figure 3.3.3a shows the skin-core-skin model created for PP-base and Figure 3.3.3b shows the model with quasi uniform fibre distribution in the direction of thickness for the other composites.



Figure 3.3.3: The developed models considering the fibre distribution in the direction of thickness

In module **Step**, seven coupled Temperature-Displacement steps with transient response has been defined. Later at the load module each of the steps will imply one environmental temperature. In field output manager by editing the field output total strain components and element temperature have been ticked.

In load module, boundary conditions have been implemented to position the specimen same as in the experimental test, Figure 3.3.4 shows the schematic of the implemented boundary condition. For each of the steps, which was created in the step module, a boundary condition from the type temperature was created. For all of the materials except PP-base materials, the simulation starting temperature is -40°C and it increases up to 200°C with an increase of 40°C in each step, for PP-base materials the simulation starting temperature is -25°C and it increases up to 150°C with an increase of 25°C in each step.

Simulation



Figure 3.3.4: Schematic of the boundary condition implemented in Abaqus

The model is discretized with hexahedral coupled Temperature-Displacement elements with a global size of 0.4 mm.

Figure 3.3.5 illustrates the simulation result performed for PEEK-GF30 at 200 °C.

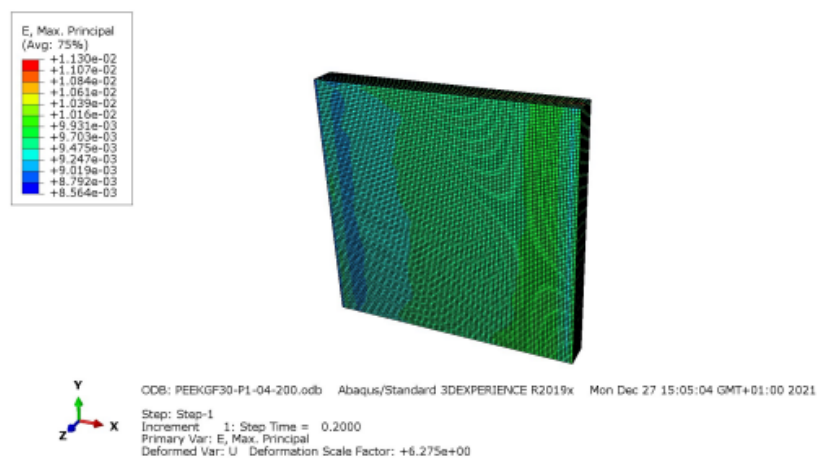


Figure 3.3.5: Thermal strains for PEEK-GF30 sample at 200 °C

Chapter 4

Results and discussion

This chapter presents the experiment results and the evaluation of the simulations. The chapter begins with a comparison between the measured specific heat capacity of the investigated composites and the theoretical calculated one. The second part of the chapter discusses the measured heat conductivities by the two methods, introduced in second chapter. This chapter ends up with a comparison between the measured and simulated thermal strains and the evaluation of the simulation.

4.1 Specific heat capacity

Specific heat capacity has been measured for each material during heating and cooling with a heating/cooling rate of 10 °C/min. Figure 4.1.1 illustrates the measured specific heat capacity of each material in a temperature interval from -25 °C up to 150 °C for PP-base materials and for the other materials from -40 °C up to 200 °C .

The glass transition for PP-base composites is not clearly in the performed DSC tests visible but for PEEK-CF30, PEEK-GF30 and PPA-GF50 the small jump in specific heat capacity curves around 140 °C shows the glass transition. Respectively, for PA6-GF50, a smooth jump in the specific heat capacity curve was observed around 70 °C , which shows the glass transition in the PA6. It is necessary to mention that the glass transition temperature of the matrix could be slightly affected by the reinforcements or additive materials, as it mentioned in several studies [66,67].

To evaluate the measured specific heat capacities, specific heat capacity of each of the composites has been theoretically calculated for room temperature, using Equation 2.1, see section 2.3. Figure 4.1.2 shows the measured and calculated specific heat capacity of the investigated materials at room

Results and discussion

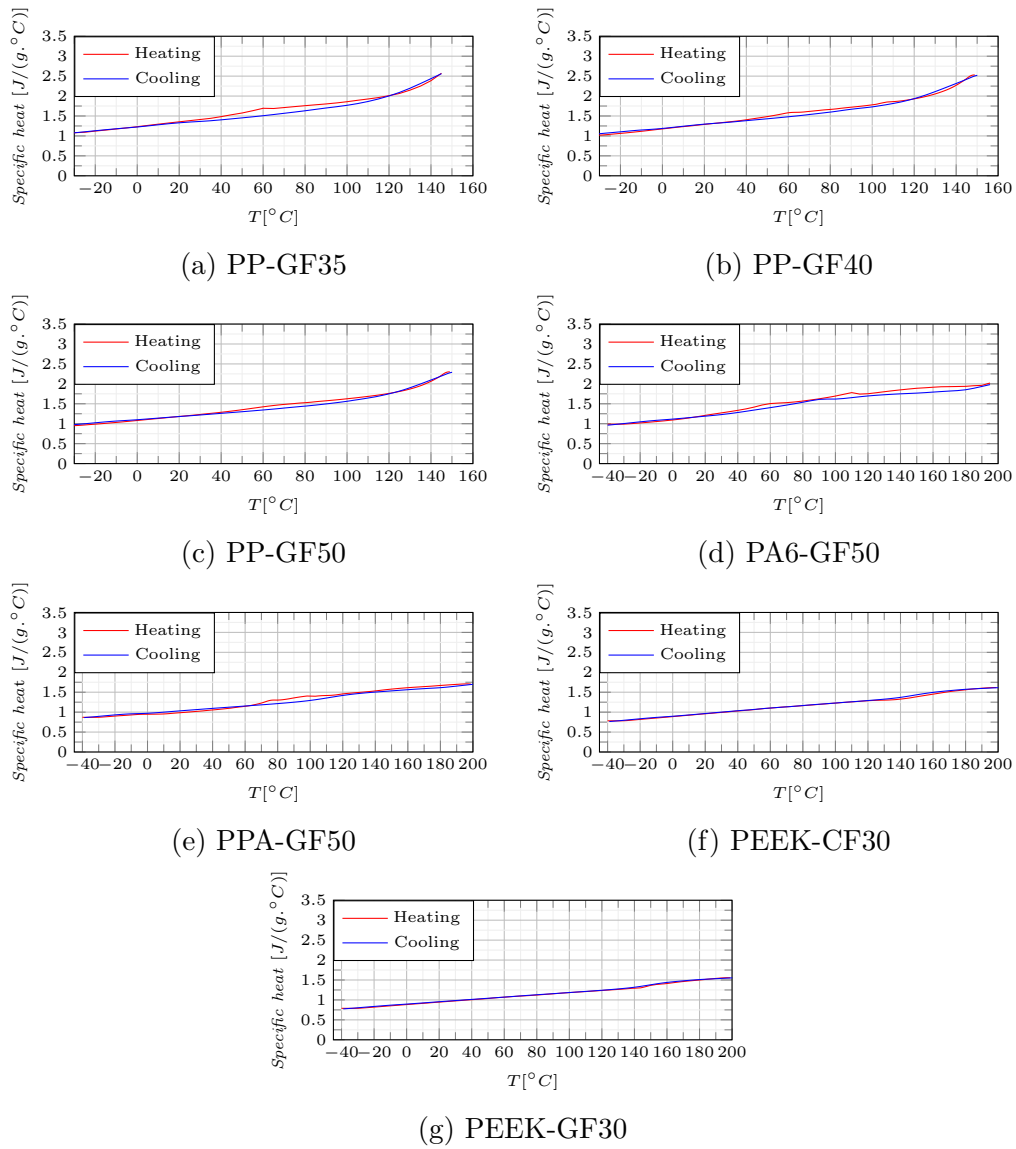


Figure 4.1.1: Measured specific heat capacity with DSC

temperature. As it could be recognized from Figure 4.1.2, the measurement results fit quite well with the calculated ones. The highest deviation between measured and calculated specific heat capacity belongs to PPA-GF50 with about 10%. The reason of this variation can be the inhomogeneity of the composites or the possible additives which are not considered in the calculations.

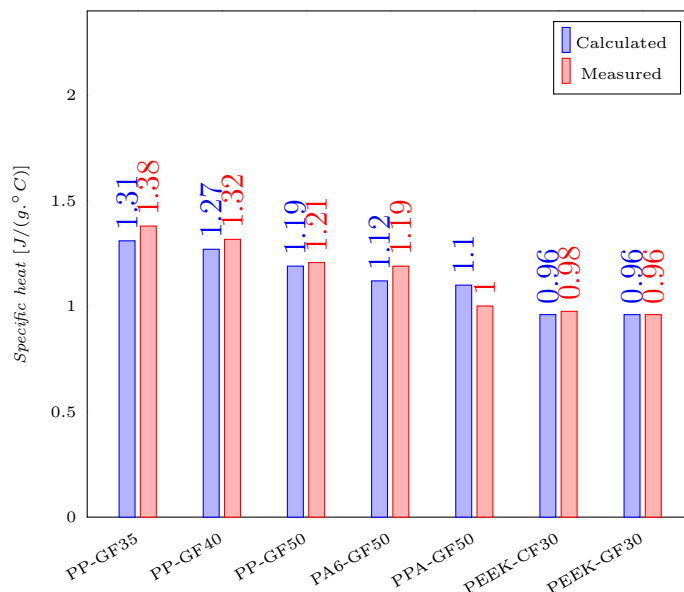


Figure 4.1.2: Comparison between measured and calculated specific heat capacity at room temperature

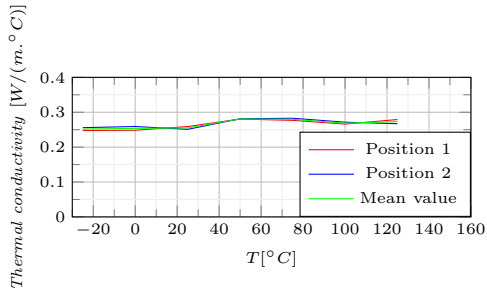
4.2 Thermal conductivity

Thermal diffusivity of each material have been measured with the same method but with two different devices. The LFA device available at PCCL can provide thermal diffusivity as a function of temperature but the setup available at the chair of Automation can just measure thermal diffusivity at room temperature. Figure 4.2.1 shows the driven thermal conductivity from the measured thermal diffusivities by LFA device for the two different positions, position 1 and position 3 in Figure 2.1.1, and the mean thermal conductivity of the two chosen positions. As it could be observed in Figure 4.2.1, there is no significant different between the driven thermal conductivities of the different positions for all of the investigated materials and thermal conductivity could be considered homogeneous. From PP-GF35 to PP-GF50, thermal conductivity increases slightly, which is due to the higher

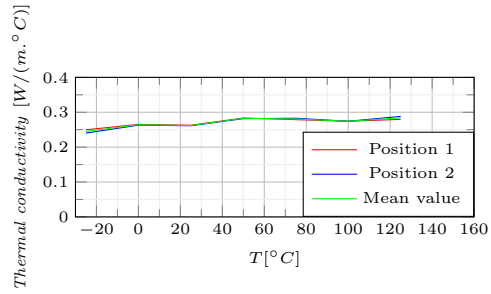
Results and discussion

thermal conductivity of glass fibre ($0.6 \text{ W m}^{-1} \text{ }^\circ\text{C}^{-1}$ [68]) in compare to PP ($0.11 \text{ W m}^{-1} \text{ }^\circ\text{C}^{-1}$ - $0.22 \text{ W m}^{-1} \text{ }^\circ\text{C}^{-1}$ [34]).

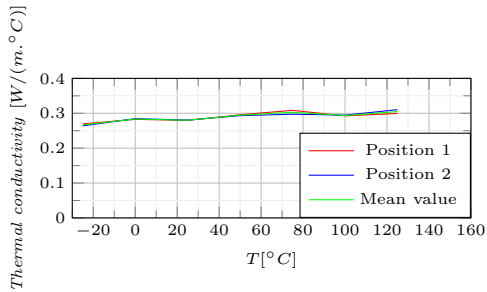
It should also be mentioned that the driven thermal conductivities are valid for the direction of thickness and thermal conductivity in the other directions will be different due to the orthotropic thermal conductivity of glass and carbon fibres. The thermal conductivity of glass fibre in longitudinal direction is about $1.2 \text{ W m}^{-1} \text{ }^\circ\text{C}^{-1}$ while thermal conductivity in transversal direction is about 50 % smaller [68]. For carbon fibre, thermal conductivity in longitudinal direction is about $8.5 \text{ W m}^{-1} \text{ }^\circ\text{C}^{-1}$ and for transversal direction about $2 \text{ W m}^{-1} \text{ }^\circ\text{C}^{-1}$ [69].



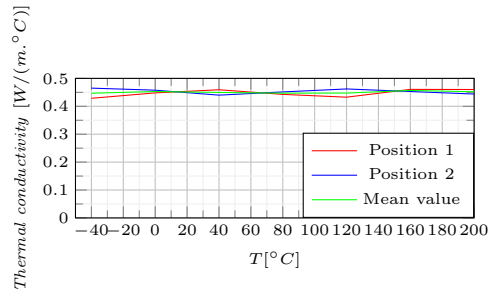
(a) PP-GF35



(b) PP-GF40



(c) PP-GF50



(d) PA6-GF50

Results and discussion

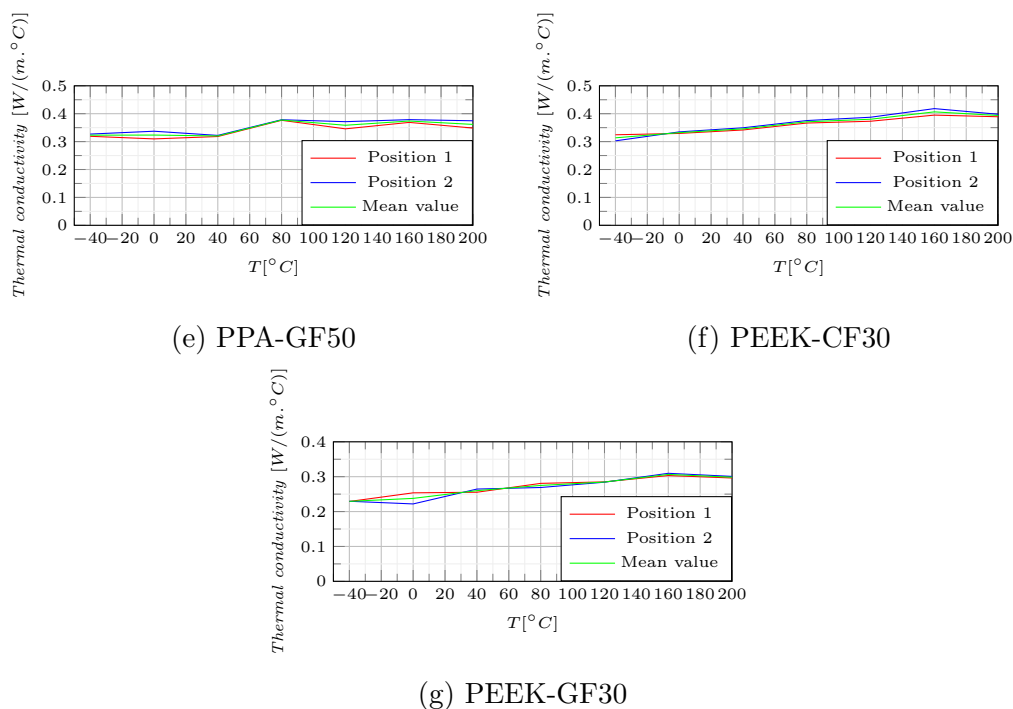


Figure 4.2.1: Driven thermal conductivity as a function of temperature

In Figure 4.2.2, the average of the driven thermal conductivity of each material from LFA and from the setup at chair of Automation at room temperature is illustrated. For all of the materials a deviation between the measured thermal conductivity by LFA and the measured thermal conductivity by the provided setup at the chair of Automation have been observed. After investigation the possible reasons for this deviation, it was concluded that the possible reason of the deviation could be the setup which have been used for placing the specimen. LFA device used a metallic cavity for placing the specimen. However, at the chair of Automation a paper made setup has been used for placing the specimen, which has clearly a lower thermal conductivity comparing with the sample holder of LFA device. Figure 4.2.3 shows the exemplary temperature change curves of the rear face of the specimen recorded by the two methods. As it shown in Figure 4.2.3 in the LFA measurements temperature falls down faster than in the other measurement method. Also, this difference in the temperature change was considered to be one reason of the systematic deviation in the measurements.

Results and discussion

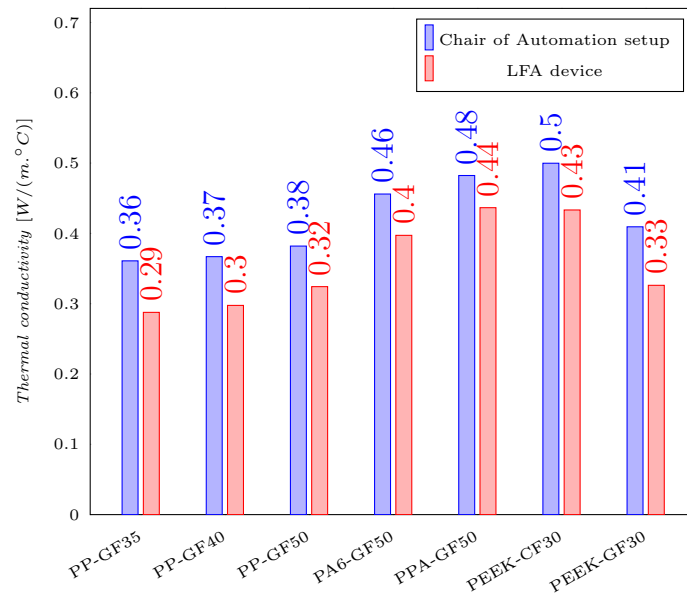
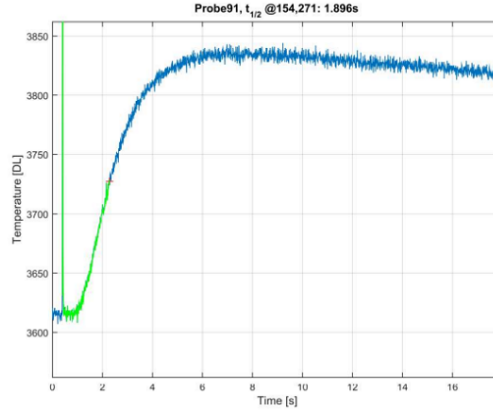
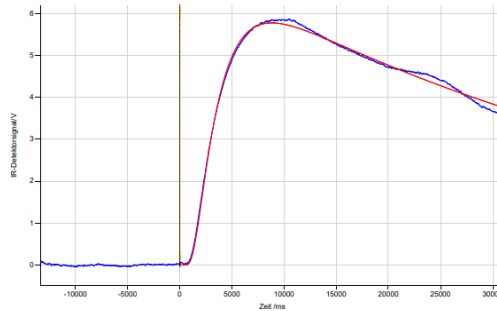


Figure 4.2.2: Average of the driven thermal conductivity from the LFA device and from the setup available at the chair of Automation at room temperature



(a) Recorded temperature changes on the rear face of the specimen by the setup at the chair of Automation



(b) Recorded temperature changes (blue line) and fitted temperature changes (red line) on the rear face of the specimen by the LFA device

Figure 4.2.3: Comparison of recorded temperature changes on the rear face of the specimen by LFA and by the setup at the chair of Automation

4.3 Thermal strain measurements and simulation validation

The method utilized for thermal strain measurements and the simulation steps have been already discussed in the second and third chapter. In this part, the results from the simulation and the results from the thermal strain measurements are presented. In all the following figures the thermal strains in the direction transversal to the mould flow direction are noticed with 'xx' and the thermal strains in the direction of mould flow are noticed with 'yy'. Figure 4.3.1 shows the comparison between the measured and simulated thermal strains for PP-base composites investigated in this thesis. As mentioned in the third chapter, since the semi-uniform fibre distribution model did not provide enough accurate estimation for the thermal strains, a skin-core-skin model for this composites has been developed and the results of this model are presented here. In the temperatures lower than zero there is a remarkable deviation between the simulation and the measured thermal strains. The possible reason for this deviation is the glass transition in PP and it seems that the simulation could not predict material behaviour around the glass transition temperature. The other point to mention is that glass transition temperature is in the optical measurements not clearly visible and measured thermal strains around glass transition temperature are changing smoothly without any sudden changes.

Results and discussion

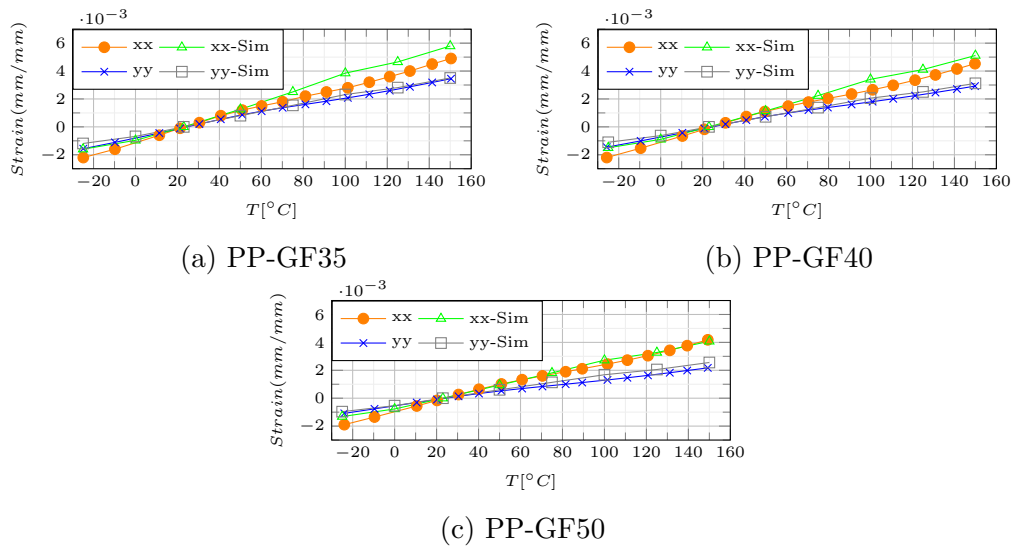


Figure 4.3.1: Measured and simulated thermal strains for PP-base composites

Figure 4.3.2 shows the simulated as well as the measured thermal strains for PA6-GF50 and PPA-GF50. The simulation model could predict the thermal strains for both PA6-GF50 and PPA-GF50 reasonably. However, for PPA-GF50 there is a certain amount of deviation between simulation and experiment around glass transition temperature.

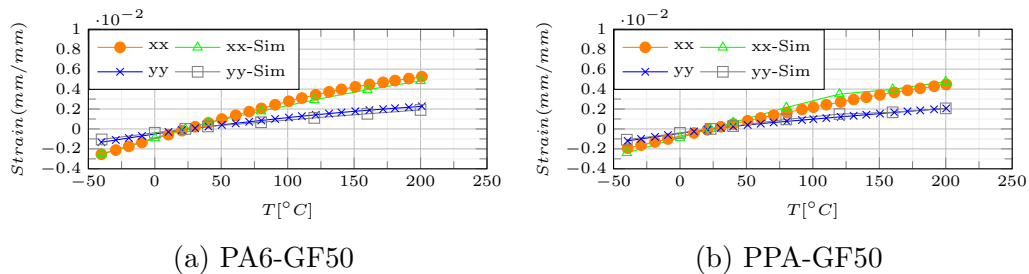


Figure 4.3.2: Measured and simulated thermal strains for PA6-GF50 and PPA-GF50

Figure 4.3.3 illustrates the measured and simulated thermal strains for PEEK-GF30 and PEEK-CF30. The thermal strains in both longitudinal and transversal directions for PEEK-CF30 are significantly less than the thermal strains of PEEK-GF30. This difference in the thermal strains is a consequence of smaller coefficient of thermal expansion of carbon fibre in compare with glass fibre. The simulation could predict thermal strains up to the glass transition temperature of PEEK (143°C) perfectly but afterward a small

Results and discussion

amount of deviation between simulation and experimental measurements was observed. On the other word, the glass transition of PEEK is in the simulation clearly remarkable. However, in the experimental measurements there is no sudden change in the measured thermal strains.

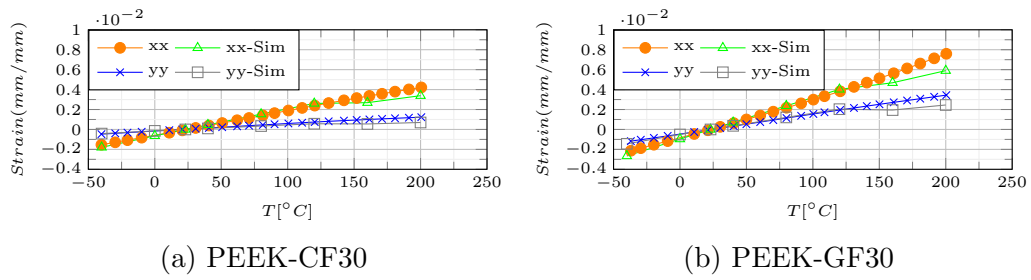


Figure 4.3.3: Measured and simulated thermal strains for PEEK-CF30 and PEEK-GF30

Chapter 5

Summary and conclusion

Polymers have in general a higher thermal expansion coefficient in compare with metals. Moreover, in short fibre reinforced polymers, the thermal expansions are direction dependent due to the nonuniform fibre orientation distribution. In many cases polymers have joints with metals and the operating temperature varies in a wide range. To avoid undesired thermal stresses, it is necessary to have an understanding from the thermomechanical behavior of the composite.

In this study Mori-Tanaka first order scheme has been utilized for material homogenization. Seven different composites have been chosen for the study. A thermomechanical simulation has been performed to predict the thermal expansions and the thermal expansions have been measured also experimentally in two directions, the expansion in the direction of thickness were neglected.

To achieve specific heat capacity of the composites as a function of temperature for the thermomechanical simulation, several DSC tests have been performed in a wide temperature range. Coefficient of thermal conductivity has been measured four times for each material by two different devices, once as a function of temperature and once in room temperature. The average value of both specific heat and thermal conductivity measurements were used for the simulation. It should also be mentioned, that no remarkable difference in the measured specific heat and measured thermal conductivity for different samples was observed.

Comparing the results from the measurements and from the simulation, it was observed that the semi-uniform fibre distribution could not predict the thermal expansions of the PP-based composites and it was necessary to develop a skin-core-skin model for predicting thermal expansions in this composites. The skin-core-skin model was also not able to predict the thermal expansions accurately around the glass transition temperature of PP.

For PA6-GF50, PPA-GF50, PEEK-CF30 and PEEK-GF30 the quasi-uniform fibre distribution model with the mapped fibre orientation from the processing simulation has been performed. The simulation provides an accurate estimation for the thermal strains of PA6-GF50 in the whole investigated temperature interval. Nevertheless, for PPA-GF50 there is a certain deviation between simulation results and measured thermal strains around the glass transition of PPA. For PEEK-CF30 and PEEK-GF30, the simulation predicts thermal expansions perfectly up to the glass transition temperature of PEEK but after the glass transition temperature the simulation underestimates thermal expansion in both directions.

Outlook

In this thesis a first order Mori-Tanaka scheme has been used for material homogenization. The E-Modulus of the matrixes are temperature dependent defined, whereas the coefficient of thermal expansion for the fibres and for all of the matrixes except PP are temperature independent defined. For future studies, the following suggestions are made:

- Using other homogenization methods to compare the efficiency of different methods
- Using the temperature dependent coefficient of thermal expansion for the both fibres and matrixes
- Validating the simulation on a real component

List of Figures

1.1.1	Microstructure of an amorphous polymer [6]	3
1.1.2	Microstructure of a semi-crystalline polymer [6]	4
1.1.3	Schematized E-Module changes vs. temperature for amorphous materials and semi-crystalline materials [9]	4
1.1.4	Classification of the thermoplastics regarding to the maximum allowed operating temperature [8]	5
1.1.5	Typical stress-strain diagram for the elastomers [3]	6
1.1.6	Schematic of the microstructure of a thermotropic LCP in solid and molten state [6]	6
1.1.7	Several types of composite materials [28]	8
1.1.8	Fiber distribution in OA_1 : flow direction, OA_2 : transverse to flow direction, OA_3 : thickness [30]	9
1.2.1	Working principle of DSC [33]	11
1.2.2	Characterization of glass transition in DSC test [32]	11
1.2.3	Flash light thermography setup	13
1.2.4	Exemplary recorded data by IR-camera	14
1.4.1	The idea of homogenization in linear elasticity [39]	15
2.1.1	Schematic of the test samples location	20
2.3.1	Used equipment for (a) weighting DSC samples and (b) for performing DSC tests	22
2.4.1	Flash light thermography setup	24
2.4.2	Flash light thermography specimen and the chosen area for calculating thermal diffusivity (green square)	24
2.4.3	Flash light thermography (a) setup and (b) principle of working	25
2.5.1	Thermal expansion measurements (a) the device used for the measurements and (b) an specimen subjected to the investigations	27
3.1.1	Working flow in Digimat	29
3.2.1	Digimat-MF general parameters	30

3.2.2 Piecewise linear function for describing PEEK Young's modulus temperature dependency	31
3.2.3 Inclusion parameters for PEEK-30GF	32
3.2.4 Digimat-MAP, Donor mesh and the structural mesh placed on it (red spot)	33
3.3.1 importing material properties to Abaqus using Digimat Plug-in	35
3.3.2 required data from .aba file, for defining the material properties in Abaqus	35
3.3.3 The developed models considering the fibre distribution in the direction of thickness	36
3.3.4 Schematic of the boundary condition implemented in Abaqus .	37
3.3.5 Thermal strains for PEEK-GF30 sample at 200 °C	37
4.1.1 Measured specific heat capacity with DSC	39
4.1.2 Comparison between measured and calculated specific heat capacity at room temperature	40
4.2.1 Driven thermal conductivity as a function of temperature . . .	42
4.2.2 Average of the driven thermal conductivity from the LFA device and from the setup available at the chair of Automation at room temperature	43
4.2.3 Comparison of recorded temperature changes on the rear face of the specimen by LFA and by the setup at the chair of Automation	44
4.3.1 Measured and simulated thermal strains for PP-base composites	45
4.3.2 Measured and simulated thermal strains for PA6-GF50 and PPA-GF50	45
4.3.3 Measured and simulated thermal strains for PEEK-CF30 and PEEK-GF30	46

List of Tables

2.1.1 List of the chosen composites for this thesis	19
2.3.1 Literature value of heat capacity for Matrix and Carbon/Glass Fiber	23
3.2.1 Thermomechanical properties of the matrix and fibre materials	30

Bibliography

- [1] Tatyana Ageyeva, Tamás Bárány, and József Karger-Kocsis. Composites. In József Karger-Kocsis and Tamás Bárány, editors, *Polypropylene Handbook*, pages 481–578. Springer International Publishing, Cham, 2019.
- [2] Michel Biron. Thermoplastics. In *Material Selection for Thermoplastic Parts*, pages 77–111. Elsevier, 2016.
- [3] Tonguç Özdemir. Elastomeric micro- and nanocomposites for neutron shielding. In *Micro and Nanostructured Composite Materials for Neutron Shielding Applications*, pages 125–137. Elsevier, 2020.
- [4] Vinny R. Sastri. High-temperature engineering thermoplastics: Polysulfones, polyimides, polysulfides, polyketones, liquid crystalline polymers, and fluoropolymers. In *Plastics in Medical Devices*, pages 175–215. Elsevier, 2010.
- [5] Arjulizan Rusli, MB.H. Othman, and K. I. Ku Marsilla. Plastics in high heat resistant applications. In *Reference Module in Materials Science and Materials Engineering*. Elsevier, 2021.
- [6] John R. Wagner, Eldridge M. Mount, and Harold F. Giles. Polymer structure. In *Extrusion*, pages 225–232. Elsevier, 2014.
- [7] ROBERT SCHIRRER. Damage mechanisms in amorphous glassy polymers: Crazing. In *Handbook of Materials Behavior Models*, pages 488–499. Elsevier, 2001.
- [8] Matthias Worgull. Molding materials for hot embossing. In *Hot Embossing*, pages 57–112. Elsevier, 2009.
- [9] Michel Biron. Thermoplastic specific properties. In *Material Selection for Thermoplastic Parts*, pages 39–75. Elsevier, 2016.

-
- [10] J.-P. Pascault and R.J.J. Williams. Overview of thermosets: Present and future. In *Thermosets*, pages 3–34. Elsevier, 2018.
- [11] Mariam Al Ali AlMaadeed, Deepalekshmi Ponnamma, and Ali Alaa El-Samak. Polymers to improve the world and lifestyle: physical, mechanical, and chemical needs. In *Polymer Science and Innovative Applications*, pages 1–19. Elsevier, 2020.
- [12] Alfréd Menyhárd, Joseph D. Menczel, and Tonson Abraham. Polypropylene fibers. In *Thermal Analysis of Textiles and Fibers*, pages 205–222. Elsevier, 2020.
- [13] G. R. Koerner, Y. G. Hsuan, and R. M. Koerner. The durability of geosynthetics. In *Geosynthetics in Civil Engineering*, pages 36–65. Elsevier, 2007.
- [14] Giovanni Talarico, Claudio de Rosa, and Finizia Auriemma. Tacticity, regio and stereoregularity. In József Karger-Kocsis and Tamás Bárány, editors, *Polypropylene Handbook*, pages 1–35. Springer International Publishing, Cham, 2019.
- [15] Nataša Z. Tomić and Aleksandar D. Marinković. Compatibilization of polymer blends by the addition of graft copolymers. In *Compatibilization of Polymer Blends*, pages 103–144. Elsevier, 2020.
- [16] Joseph P. Greene. Microstructures of polymers. In *Automotive Plastics and Composites*, pages 27–37. Elsevier, 2021.
- [17] Vinny R. Sastri. Engineering thermoplastics. In *Plastics in Medical Devices*, pages 121–173. Elsevier, 2010.
- [18] R. Rulken and C. Koning. Chemistry and technology of polyamides. In *Polymer Science: A Comprehensive Reference*, pages 431–467. Elsevier, 2012.
- [19] Ayesha Kausar. Physical properties of hybrid polymer/clay composites. In *Hybrid Polymer Composite Materials*, pages 115–132. Elsevier, 2017.
- [20] R. Greco and L. Nicolais. Glass transition temperature in nylons. *Polymer*, 17(12):1049–1053, 1976.
- [21] Sina Ebnesajjad and Richard A. Morgan. Fluorinated Additives for Plastics. In *Fluoropolymer Additives*, pages 107–148. Elsevier, 2012.

-
- [22] Laurence W. McKeen. Polyamides (nylons). In *The Effect of UV Light and Weather on Plastics and Elastomers*, pages 185–222. Elsevier, 2019.
- [23] Akro Plastic. High temperature nylons. <https://akro-plastic.com/compound-overview/akromid-t/>, 2022; Online; accessed 07-April-2022.
- [24] Laurence W. McKeen. High-temperature polymers. In *The Effect of Creep and Other Time Related Factors on Plastics and Elastomers*, pages 337–372. Elsevier, 2009.
- [25] Ohan S. Manoukian, Naseem Sardashti, Teagen Stedman, Katie Gailunas, Anurag Ojha, Aura Penalosa, Christopher Mancuso, Michelle Hobert, and Sangamesh G. Kumbar. Biomaterials for tissue engineering and regenerative medicine. In *Encyclopedia of Biomedical Engineering*, pages 462–482. Elsevier, 2019.
- [26] P. A. Gunatillake and R. Adhikari. Nondegradable synthetic polymers for medical devices and implants. In *Biosynthetic Polymers for Medical Applications*, pages 33–62. Elsevier, 2016.
- [27] Donald G. Baird. Polymer processing. In *Encyclopedia of Physical Science and Technology*, pages 611–643. Elsevier, 2003.
- [28] Laurence W. McKeen. Introduction to plastics and polymers. In *Fatigue and Tribological Properties of Plastics and Elastomers*, pages 45–64. Elsevier, 2016.
- [29] Shao-yun Fu, Bernd Lauke, and Yiu-wing Mai. Introduction to short fibre-reinforced polymer composites. In *Science and Engineering of Short Fibre-Reinforced Polymer Composites*, pages 1–7. Elsevier, 2019.
- [30] A. Dean, S. Sahraee, J. Reinoso, and R. Rolfes. A new invariant-based thermo-plastic model for finite deformation analysis of short fibre reinforced composites: Development and numerical aspects. *Composites Part B: Engineering*, 125:241–258, 2017.
- [31] Gabriel Stadler, Andreas Primetzhofer, Gerald Pinter, and Florian Grün. Investigation of fibre orientation and notch support of short glass fibre reinforced thermoplastics. *International Journal of Fatigue*, 131:105284, 2020.
- [32] Joseph D. Menczel, Lawrence Judovits, R. Bruce Prime, Harvey E. Bair, Mike Reading, and Steven Swier. Differential scanning calorimetry (dsc).

-
- In Joseph D. Menczel and R. Bruce Prime, editors, *Thermal Analysis of Polymers*, pages 7–239. John Wiley & Sons, Inc, Hoboken, NJ, USA, 2009.
- [33] Joseph D. Menczel and R. Bruce Prime, editors. *Thermal Analysis of Polymers*. John Wiley & Sons, Inc, Hoboken, NJ, USA, 2009.
- [34] Antonella Patti and Domenico Acierno. Thermal conductivity of polypropylene-based materials. In Weiyu Wang and Yiming Zeng, editors, *Polypropylene - Polymerization and Characterization of Mechanical and Thermal Properties*. IntechOpen, 2020.
- [35] Y. Huang. Electrical and thermal properties of activated carbon fibers. In *Activated Carbon Fiber and Textiles*, pages 181–192. Elsevier, 2017.
- [36] Numan Yüksel. The review of some commonly used methods and techniques to measure the thermal conductivity of insulation materials. In Amjad Almusaed and Asaad Almssad, editors, *Insulation Materials in Context of Sustainability*. InTech, 2016.
- [37] W. J. Parker, R. J. Jenkins, C. P. Butler, and G. L. Abbott. Flash method of determining thermal diffusivity, heat capacity, and thermal conductivity. *Journal of Applied Physics*, 32(9):1679–1684, 1961.
- [38] Nick McCormick and Jerry Lord. Digital image correlation. *Materials Today*, 13(12):52–54, 2010.
- [39] Ex-stream Engineering. Digimat.2021: User documentation.
- [40] J. C. Halpin Affdl and J. L. Kardos. The halpin-tsai equations: A review. *Polymer Engineering and Science*, 16(5):344–352, 1976.
- [41] T. Mori and K. Tanaka. Average stress in matrix and average elastic energy of materials with misfitting inclusions. *Acta Metallurgica*, 21(5):571–574, 1973.
- [42] Pattabhi Ramaiah Budarapu, Xiaoying Zhuang, Timon Rabczuk, and Stephane P.A. Bordas. Multiscale modeling of material failure: Theory and computational methods. In *Advances in Crystals and Elastic Metamaterials, Part 2*, volume 52 of *Advances in Applied Mechanics*, pages 1–103. Elsevier, 2019.
- [43] J. D. Eshelby. The determination of the elastic field of an ellipsoidal inclusion, and related problems. *Proceedings of the Royal Society of*

-
- London. Series A. Mathematical and Physical Sciences*, 241(1226):376–396, 1957.
- [44] Shao-yun Fu, Bernd Lauke, and Yiu-wing Mai. Thermal conductivity and expansion of short fibre-reinforced polymer composites. In *Science and Engineering of Short Fibre-Reinforced Polymer Composites*, pages 213–240. Elsevier, 2019.
- [45] G. R. Liu and S. S. Quek. Fundamentals for finite element method. In *The Finite Element Method*, pages 43–79. Elsevier, 2014.
- [46] Wasim Younis. The stress analysis environment. In *Up and Running with Autodesk Inventor Simulation 2011*, pages 235–275. Elsevier, 2010.
- [47] Marshall Bern and Paul Plassmann. Mesh generation. In *Handbook of Computational Geometry*, pages 291–332. Elsevier, 2000.
- [48] Dassault Systemes. Abaqus: User manual.
- [49] Borealis GmbH. Product data sheet - polypropylene. <https://www.borealisgroup.com/product/fibremod-gb477hp/data-sheets?context=https://www.borealisgroup.com&search-global-search&index-search=products&id-search=28402>, Online; accessed 07-April-2022.
- [50] Campus plastics. Datasheet - grilon tsg-50/4 w. <https://www.campusplastics.com/campus/de/datasheet/Grilon+TSG-504+W/EMS-GRIVORY+%7C+a+unit+of+EMS-CHEMIE+AG/61/6c9bce0f>, Online; accessed 07-April-2022.
- [51] Campus plastics. Datasheet - grivory htv-5h1 black 9205. <https://www.campusplastics.com/campus/de/datasheet/Grivory+HTV-5H1+black+9205/EMS-GRIVORY+%7C+a+unit+of+EMS-CHEMIE+AG/61/bd11ffb8>, Online; accessed 07-April-2022.
- [52] Ensinger Plastics. Tecapeek cf30 black. <https://www.ensingerplastics.com/en/shapes/products/peek-tecapeek-cf30-black>, Online; accessed 07-April-2022.
- [53] Plastmass Group. What is peek gf30? <https://www.plastmass-group.com/post/what-is-peek-gf30>, Online; accessed 07-April-2022.

-
- [54] Md. Amir Sohel, Arunava Mandal, Abhijit Mondal, Sandip Pan, and Asmita SenGupta. Thermal analysis of abs/pa6 polymer blend using differential scanning calorimetry. *Journal of Thermal Analysis and Calorimetry*, 129(3):1689–1695, 2017.
- [55] Bernd Weidenfeller, Michael Höfer, and Frank R. Schilling. Thermal conductivity, thermal diffusivity, and specific heat capacity of particle filled polypropylene. *Composites Part A: Applied Science and Manufacturing*, 35(4):423–429, 2004.
- [56] Make It Form. Polyphthalamide (ppa). <https://www.makeitfrom.com/material-properties/Polyphthalamide-PPA>, Online; accessed 07-April-2022.
- [57] Lisa Rivière, Nicolas Caussé, Antoine Lonjon, Éric Dantras, and Colette Lacabanne. Specific heat capacity and thermal conductivity of peek/ag nanoparticles composites determined by modulated-temperature differential scanning calorimetry. *Polymer Degradation and Stability*, 127:98–104, 2016.
- [58] Azo Materials. E-glass fibre. <https://www.azom.com/properties.aspx?ArticleID=764>, Online; accessed 07-April-2022.
- [59] Azo Materials. Carbon - graphite materials. <https://www.azom.com/properties.aspx?ArticleID=516>, Online; accessed 07-April-2022.
- [60] NETZSCH. LFA 467 HyperFlash. <https://www.netzsch-thermal-analysis.com/de/produkte-loesungen/waerme-und-temperatur-leitfaehigkeitsbestimmung/lfa-467-hyperflash/>, 2022; Online; accessed 07-April-2022.
- [61] DANTEC. Solid mechanics dic. <https://www.dantecdynamics.com/solutions-applications/solutions/stress-strain-espi-dic/digital-image-correlation-dic/>, Online; accessed 07-April-2022.
- [62] Mohammed Alsalihi. *Mechanical Properties of Glass Fiber Reinforced Polymer Bars After Exposure to Elevated Temperatures*. PhD thesis, 12 2014.
- [63] Chaoyong Li, Rongtao Zhu, Huang Pengfei, and Xian Wang. Interfacial shear strength and fracture toughness between single carbon fiber and tio 2 matrix under microbond test. *The Journal of Adhesion*, 97:1–19, 12 2019.

-
- [64] Andreas Primetzhofer, Gabriel Stadler, Gerald Pinter, and Florian Grün. Lifetime assessment of anisotropic materials by the example short fibre reinforced plastic. *International Journal of Fatigue*, 120:294–302, 2019.
- [65] François Trochu, Edu Ruiz, Vincent Achim, and Sofiane Soukane. Advanced numerical simulation of liquid composite molding for process analysis and optimization. *Composites Part A: Applied Science and Manufacturing*, 37(6):890–902, 2006.
- [66] Craig Clemons and Anand R. Sanadi. Instrumented impact testing of kenaf fiber reinforced polypropylene composites: Effects of temperature and composition. *Journal of Reinforced Plastics and Composites*, 26(15):1587–1602, 2007.
- [67] Ludwig Rebenfeld, Glenn P. Desio, and James C. Wu. Effects of fibers on the glass transition temperature of polyphenylene sulfide composites. *Journal of Applied Polymer Science*, 42(3):801–805, 1991.
- [68] C. H. Zweben. Composites: Overview. In *Encyclopedia of Condensed Matter Physics*, pages 192–208. Elsevier, 2005.
- [69] Damien Lecointe, Maxime Villière, Sawsane Nakouzi, Vincent Sobotka, Nicolas Boyard, Fabrice Schmidt, and D. Delaunay. Experimental determination and modeling of thermal conductivity tensor of carbon/epoxy composite. *Key Engineering Materials*, 504-506:1091–1096, 2012.